



D I P L O M A R B E I T

Adaptives Filter zur Positionsbestimmung eines Positronenemitters in einer neuartigen PET/MRT-Kopfspule

Ausgeführt am

Institut für Angewandte Physik
der Technischen Universität Wien

In Zusammenarbeit mit dem
Zentrum für medizinische Physik und biomedizinische Technik
der Medizinischen Universität Wien

Unter der Anleitung von:

Ao.Univ.Prof. Dipl.-Ing. Dr.techn. Martin Gröschl

Und unter Mitbetreuung von:

Ao.Univ.Prof. Univ.Doz. Mag. Dr. Wolfgang Birkfellner

durch

Mathias Glanzer

Sankt Anna Straße 27

A-9081 Reifnitz am Wörthersee

September 11, 2017

Abstract

In PET/MRI an attenuation map for the PET cannot be obtained directly by the MRI data. At the moment different MRI-based segmentation methods are available but none of them leads to satisfying results. Therefore a new idea came up with the aim to achieve an attenuation map via a transmission-based (Tx-based) segmentation. A head coil system was developed which allows to move a transmission source within a liquid drive around the patient. To use the data obtained by this source, its location has to be known at any time. An MRI-compatible lightbarrier system has the possibility to track the pellet within the hydraulic drive on defined spots. As the motion of the point source is not consistent due to different effects, a program should provide information about the location at any time of the scan. The experiments showed that especially the filling of the point source has an influence on its movement. The developed program considers this effect by calculating different correction factors for different parts of the liquid drive.

Kurzfassung

Die Abschwächungskorrektur für ein PET kann bei einem PET/MRT nicht direkt aus den MRT-Daten gewonnen werden. Neben verschiedenen MRT-basierten Lösungen, welche bisweilen nicht zu zufriedenstellenden Ergebnissen geführt haben, kam eine neue Idee auf, welche auf einer zusätzlichen Transmissionsquelle beruht (Tx-basiert). Dafür wurde eine PET/MRT-Kopfspule entwickelt, die eine spiralförmige Bewegung einer solchen Quelle in einem Schlauchsystem um den Patienten erlaubt. Um die erhaltenen Daten für die Abschwächungskorrektur nützen zu können, muss jedoch jederzeit die Position dieser Quelle bekannt sein. Mit Hilfe eines MRT-kompatiblen Lichtschrankensystems ist es möglich die Transmissionsquelle an bestimmten Punkten zu orten. Basierend auf dieser Grundlage wurde ein Programm entwickelt, das Informationen über den Aufenthaltsort für jeden Zeitpunkt eines Scans bereitstellt. In Experimenten wurde beobachtet, dass vor allem das eingefüllte Volumen in diese Quelle Einfluss auf die Bewegung hat. Das Programm berechnet daher verschiedene Korrekturfaktoren für die Geschwindigkeit, abhängig von der aktuellen Position im Schlauchsystem.

Contents

1	Introduction	1
2	Theory and background	3
2.1	PET	3
2.2	MRI	6
2.3	Hybrid imaging and PET/MRI	8
2.4	Attenuation correction	9
2.5	Fundamentals of fluid mechanics	11
2.6	Adaptive filter	14
2.7	PET/MRI head coil	15
2.8	Lightbarrier	16
2.9	Qt	19
2.9.1	Qt Designer	19
2.9.2	Qt-Creator	20
3	Materials and methods	21
3.1	Liquid drive	21
3.1.1	Voltage source	21
3.1.2	Pump	22
3.1.3	Tube system	23
3.2	Pellet	27
3.3	Lightbarrier system	30
3.4	Program and Filter	32
4	Results and Discussion	37
4.1	Voltage/Time relation	37
4.2	Loss of pressure in the liquid drive	40
4.3	Filling of the pellet	43
4.4	Movement within one round	48
4.5	Consistency of round time	52
4.6	Loss of water	54
4.7	Lightbarrier manual	55

Contents

5 Conclusion and Outlook	61
6 Acknowledgments	63
Bibliography	65
List of Figures	67
List of Tables	71
List of Abbreviations	73
A Appendix	75
A.1 Time/Voltage comparison	75
A.2 Filling	77
A.3 Quarter coefficients	80
A.4 Round movement	83
A.5 Code segments	86
A.5.1 MuckData	86
A.5.2 Output Data	88

1 Introduction

Hybrid imaging techniques are more and more requested in modern medicine. In oncology positron emission tomography (PET) is an important tool to diagnose a tumor. Without any further imaging technique, linking the detected metabolic information with the anatomy of the patient is a delicate task. This information has to be provided by other imaging techniques as computer tomography (CT) or magnetic resonance imaging (MRI). While PET/CT is already commonly used, PET/MRI is still in the development phase. The main hurdle is attenuation correction (AC) as an attenuation map cannot be obtained directly from the MRI data. Several groups [1, 2, 3] have already dealt with this problem.

This thesis is part of a FWF project called *Design, Development and Validation of an Integrated Transmission Source System for PET Attenuation Correction in PET/MRI Imaging* which aims to develop a PET/MRI head coil including a transmission-based (Tx-based) attenuation correction [4]. Therefore, it revitalizes an idea of Jones et al. [5], using a radioactive point source which moves in a helical path around the patient using a hydraulic drive. The MRI-hardware of this head coil system was developed by Navarro de Lara et al. [6]. This system is a receiver coil and can be connected to a Siemens PET/MRI scanner. The hydraulic drive, developed by Renner et al. [7], consists of a hose surrounding this head coil wherein the transmission source is moving. To receive proper results for AC, the location of this point source has to be known. Therefore a lightbarrier system described in [8] is used. (Fig. 1.1)

The aim of this thesis is to describe the characteristic of the motion and the tracking of the point source in the hydraulic drive. With the aid of the lightbarrier system the source can be identified at 16 spots in the liquid drive. Starting from this information a program should be developed to determine time and position in regions between the detected spots. Furthermore the lightbarrier system has to be synchronized with the computer to receive information over the remaining dose in the point source. Beside development work, the hydraulic system should be tested during this thesis to improve it as well as the software of the lightbarrier system. Additional experiments provide basic information for further use.

1 Introduction

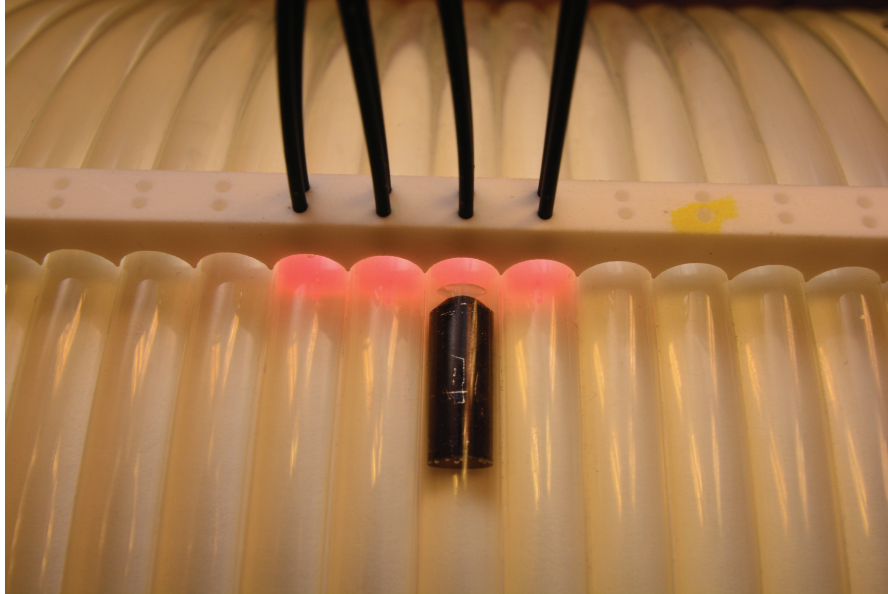


Figure 1.1: Tracking of the point source in the liquid drive

In the next chapter the theory and background of this thesis will be explained. Chapter 3 deals with the materials and methods used and developed for this work. It contains information about the parts of the liquid drive as well as considerations regarding the development of the point source and part of code developed from the lightbarrier software. The results are presented in Chapter 4. The main parts are the relation between the voltage and the go-through time as well as the loss of pressure within the liquid drive. Furthermore the motion is described and finally a manual of the developed program is given in this part. The last chapter gives an overview about the state of the whole project and an outlook on further tasks.

2 Theory and background

This chapter will give a short overview on the theoretical modalities used in this project. It will describe the imaging process of PET, MRI and their combination (PET/MRI) as well as the challenges concerning the attenuation correction. In addition it will explain theoretical details of the hydraulic system. Another section will deal with the idea of an adaptive filter and shows how it works. In the last sections the design of the PET/MRI head coil will be explained as well as the lightbarrier device used for the transmission source tracking.

2.1 PET

The aim of positron emission tomography (PET) is to image metabolic actions in the human body, which makes it an important tool in oncology. A PET scan is applied to detect or stage a tumor. It requires a radio-pharmaceutical which is in the case of this project mainly fluorodeoxyglucose (FDG), a sugar quite similar to glucose. In this tracer the stable ^{19}F is replaced by the positron emitter ^{18}F with a half life of 109,2 min. It is injected and incorporated by cells with high energy uptake. As cancer cells have a faster metabolism and therefore a higher need of sugar, FDG is mainly found in those cells where it is trapped. [9]

In a positron emitter a proton turns into a neutron plus a positron and an electron neutrino



In the case of ^{18}F used in the project this leads to



The ^{18}F atom of the sugar turns into a heavy oxygen atom which is stable again. When the reaction starts, a positron is emitted and as the atom is negatively charged after the decay, also an electron leaves the outer shell. The positron has now different ways to lose its kinetic energy:

2 Theory and background

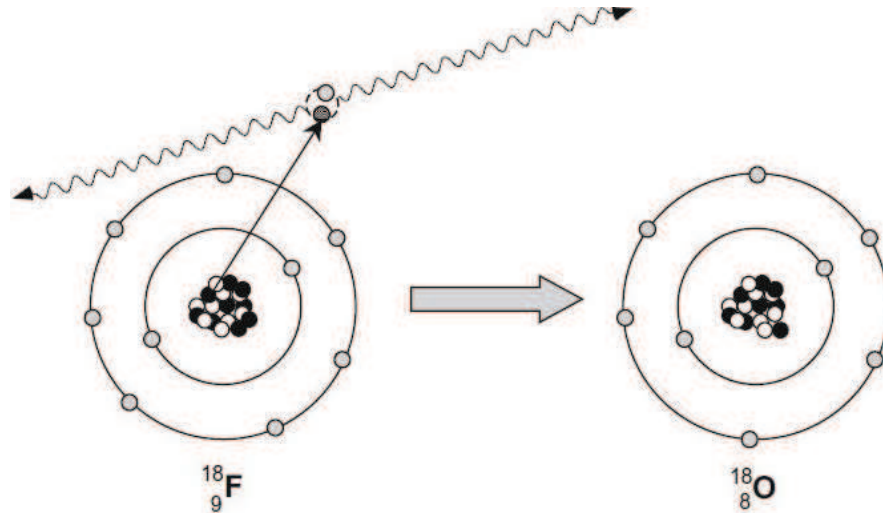


Figure 2.1: Nuclear decay of ${}^{18}\text{F}$ and electron-positron annihilation of the emitted positron. When emitted by the nucleus the positron starts to lose energy by interactions with other particles until it comes to a resting state. Then it annihilates with an electron to give rise to two photons with an energy of 511 keV each. The photons travel in approximately anti-collinear direction from the annihilation point. [9]

- inelastic collisions with electrons which leads to the main loss of kinetic energy of the positron,
- elastic scattering with electrons, here the energy and momentum is conserved only the direction is changed,
- inelastic scattering with the nucleus, which leads to Bremsstrahlung and a deflected positron and
- elastic scattering with the nucleus without any transfer of energy but a change in direction of the positron.

When the positron has lost its energy, it can annihilate with an electron leading to the production of two 511 keV photons which leave the point of annihilation in anti-collinear direction (Fig. 2.1). These photons arrive as a coincidence pair at the detector. [9]

Ideally the photons travel through the surrounding matter in a straight way, but in most cases they interact somehow and get lost. The most important interactions of the photon are:

- Photoelectric effect: An electron absorbs the photon and gets enough energy to leave the atom.

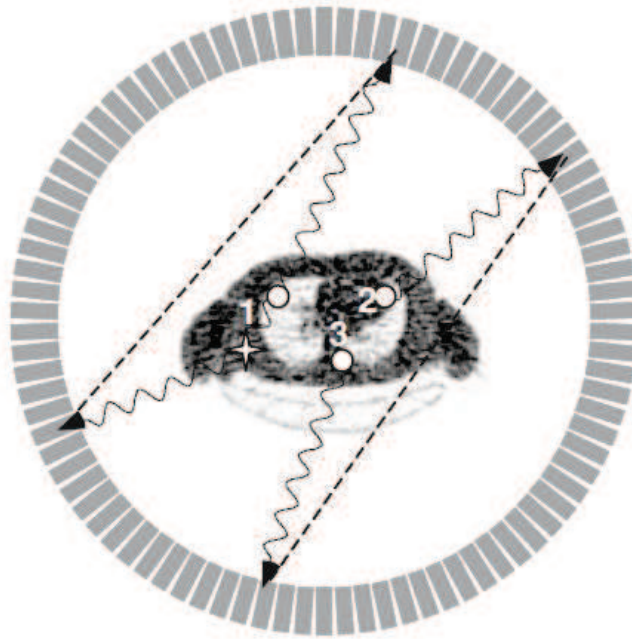


Figure 2.2: Cross section of a detector ring with a scattered and a random coincidence. One photon of event 1 is scattered which leads to a wrong LOR (dotted line). Event 2 and event 3 are unrelated but result in a LOR as long as they arrive in a coincidence timing window because one photon of each event gets lost.

- Compton scattering: A photon hits an electron and transfers a part of its energy to the electron. Furthermore the photon is deflected while the electron is able to leave the atom.

Other rare interactions are coherent scattering and the nuclear photo-absorption. Together these effects lead to a reduced signal for the PET image as less true photon pairs arrive at the detector. The term 'true photon pair' means the detection of two photons from the same annihilation point, which are not scattered or absorbed on their path. The probability of being absorbed or deflected by a material is given by the attenuation correction which is discussed in detail in Section 2.4.

The detector is arranged in ring form and consists of many small scintillators. The coincidence timing window is in a range of 10 ns, which means if two photons arrive at the detector within this time a signal is registered. After detection of two simultaneous photons a line of response (LOR) is determined. Scattered photons or the detection of two single events, where each of two unrelated events within the coincidence time window loses one photon, lead to wrong LOR (Fig. 2.2). Beside the coincidence time, energy resolution is taken into account to dispose a wrong LOR. Detectors with a lower energy gate slightly smaller than 511 keV allow to dismiss scattered photons due to their energy loss when scattered. Only true photon pairs may be taken into account for reconstruction. In addition, the

2 Theory and background

Tissue	$\mu(511 \text{ keV}) [\text{cm}^{-1}]$
Adipose tissue	0.090
Water	0.095
Lung	0.025-0.04
Smooth muscle	0.101
Cortical bone	0.178

Table 2.1: Comparison of attenuation coefficients μ for 511 keV photons in different tissue [9]

path of the positron before it has lost its energy must be considered as it leads to the resolution of PET. The free path length of the positron to lose all its kinetic energy is up to 4 mm.

The probability for a photon to be scattered or absorbed is determined by the material. This leads to different attenuation for every LOR. To develop an attenuation map attenuation coefficients of the material have to be known. Table 2.1 lists some linear attenuation coefficients μ of important tissue parts in human body. Due to differences in those coefficients the main challenge of PET is to provide an accurate attenuation map. Especially the big difference of bone and air is of relevance in PET/MRI as it will be described in Section 2.4.

2.2 MRI

The second imaging technique used in this project is magnetic resonance imaging (MRI). This imaging technique relies on the nuclear spin of atoms and molecules, mainly hydrogen, in the body. It uses the fact that particles with a net spin absorb photons with a specific frequency, the Larmor frequency ν , when they are placed in a magnetic field B . The Larmor frequency is given by

$$\nu = \gamma \cdot B \quad (2.3)$$

where γ is the gyro-magnetic factor which is specific for every substance. For protons which are the commonly nuclei used in biomedical imaging applications γ is 42.58 MHz per Tesla (T) [10] which means the Larmor frequency in a one Tesla MRI is 42.58 MHz.

The main elements of an MRI are a solenoid producing a static magnetic field, gradient coils and a radio-frequency (RF) system. The static magnet is a superconducting magnet which builds a homogeneous static magnetic field via a large coil. This field aligns the spins in z-direction. [11]

The gradient coil superimposes this magnetic field in all three directions of space. The gradients must be stronger than local field inhomogeneities of the static magnetic field but are in total much smaller than the static field itself. It is responsible for a difference of the size of the resulting magnetic field, depending on the position. This means the resulting magnetic field has the size of the static magnetic field only in one position and is bigger than it at one end and smaller at the other end. Due to the frequency dependence of the photon absorption, the gradient coil is responsible for slice selection. Varying the Larmor frequency leads to approaching of different slices because of different magnetic fields. The thickness of the selected slice depends on the one hand on the steepness of the gradient and on the other hand on the bandwidth of the RF-pulse. To receive a thin slice the bandwidth should be small while the gradient should be steep. [11]

The third component of the MRI is the RF-system, which applies energy to the spins. Higher energy leads to a higher tilt angle of the spins. Once the spins are out of the initial order the RF-pulse is turned off and the free induction decay (FID) leads to a realignment of the spins towards the initial field by transferring the absorbed energy to the surrounding. There are two specific relaxation times for every substance - the spin-lattice relaxation time T_1 and the spin-spin relaxation time T_2 . To get T_1 the applied pulse is in opposite direction to the static field. The magnetization can be saturated resulting in a net magnetization equal to 0. Afterwards, turning off the RF-pulse spins start to realign towards the initial magnetic field and the time needed for approximately 63% to return to the equilibrium state is called spin-lattice relaxation time T_1 .

$$M_Z = M_0 \cdot (1 - e^{-t/T_1}) \quad (2.4)$$

To obtain T_2 , the pulse is applied in XY-direction and again the time is measured how long it takes for approximately 63 % to return to equilibrium state.

$$M_{XY} = M_{XY_0} \cdot e^{-t/T_2} \quad (2.5)$$

T_2 depends on the molecular interactions as well as on field inhomogeneities of the magnetic field B_0 which leads to an effective time constant T_2^* . To get rid of these inhomogeneities, an 180° pulse is applied after a certain time period τ leading to an 180° turn of the net magnetization. As inhomogeneities are constant in time and space the spins recover after a further period of τ . In addition, a further signal, the echo time TE, can be measured.

$$TE = 2\tau \quad (2.6)$$

The amplitude of the spin-echo decreases with longer echo times. During the mea-

2 Theory and background

surement of the spin-echo a frequency encoding gradient is applied perpendicular to the slice encoding gradient. Spins along the gradient start to precess with different frequencies. After recording these frequencies, reconstruction of each location along the gradient can be done by using the Fourier transform. [11]

As hydrogen is bonded to different substances and is present in different concentrations in the body, those two time constants vary with the material. Due to this fact, both time constants can be used to receive a contrast in an image. Overall MRI is a technique to image soft tissue but bone and air segmentation is difficult. This disadvantage leads to big problems in PET/MRI because there is a big difference in the attenuation coefficient in PET, described in detail in Section 2.4.

2.3 Hybrid imaging and PET/MRI

Hybrid imaging means the combination of two or more different imaging modalities. In PET, it is only possible to show where the metabolism takes place without any further indication. In the beginning when PET only scanners were installed, a transmission scan was made to obtain an attenuation map. Additionally, for the anatomical information of the patient a CT was taken. Images were taken subsequently, which led to differences if it was not exactly the same position or even worse if the shape or size of the regarded object changed. To avoid this problem, PET/CT was developed to image a patient within a shorter time and in one device. In this machine first a CT and subsequently a PET is taken. Although this allowed to visualize the anatomical location of a lesion, disadvantages of CT such as bad soft tissue contrast and exposure to radiation still exist. It is also not possible to take a CT and a PET simultaneously and according to this, artifacts from movement or breathing appear [12].

The main hurdle in PET/MRI has been the compatibility of the PET-detector with the high magnetic field of the MRI. Another main challenge is the avoidance of interactions between the electronic signals of PET and the RF signals of MRI. Currently, three different ways of PET/MRI (Fig. 2.3) exist. While option (a) has the advantage of not exposing the PET detector to the magnetic field of the MRI it has the lack of possibility to take images simultaneously. Additionally acquisition time is longer than in PET/CT because a MRI lasts longer than a CT. In (b) a PET insert is used, which is positioned between the RF-coil and the gradient system of the MRI. As a standard MRI system can be used here, cost efficiency is given but due to a lack of space, such a system is of restricted usability. It can only be used for animal and brain studies. The third option is to fully integrate a

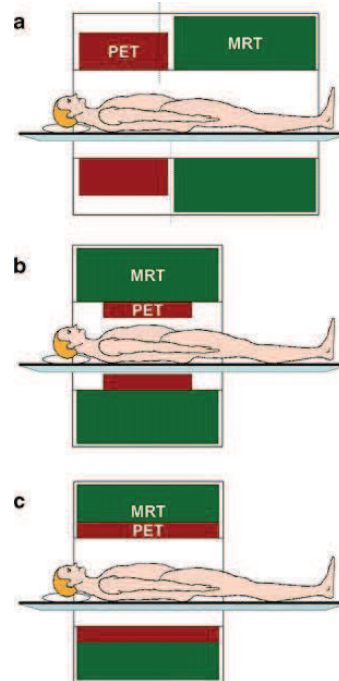


Figure 2.3: Different options of implementing a PET detector in a MRI [12]

PET-scanner into a MRI. Images are taken simultaneously and it is also possible to do whole body scans.

None of these methods mentioned above can provide an ideal attenuation correction method due to the lack to differentiate between bone and air in MRI. Therefore an idea presented by Jones et al. [5] over 20 years ago is revitalized in a FWF project. Here, a radioactive point source moves in a helical path in a so called liquid drive around the patient. Information about the location of the point source and the raw transmission data lead to an attenuation correction of the PET-image. It should combine the advantage of PET/CT of receiving an ideal attenuation map while imaging the metabolism via PET with the advantages of MRI. [5]

2.4 Attenuation correction

As illustrated before not every photon reaches the detector in direct path. Photons are scattered or absorbed on their way to the detector which leads to a reduced number of counts. The number of detected coincidences C is given by

$$C = C_0 \cdot e^{-\mu \cdot D} \quad (2.7)$$

2 Theory and background

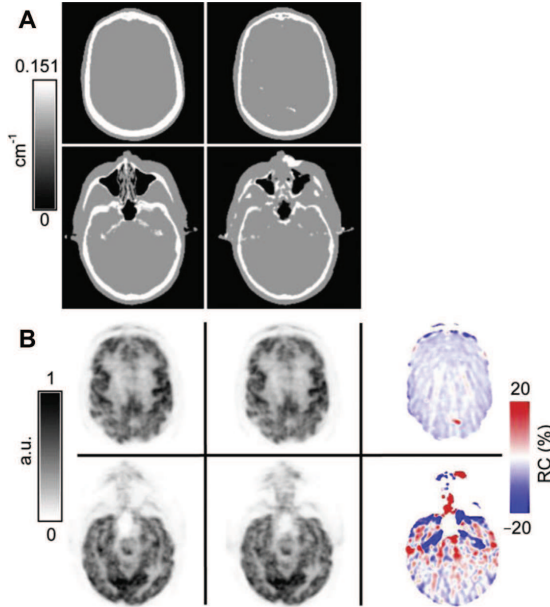


Figure 2.4: (A) Comparison of μ -maps between a CT (left) and an ultrashort echo time based MRI (right) and (B) the corresponding PET-image reconstruction. On right side in (B) a comparison of those two methods and their relative change (RC) is visualized. [2]

where C_0 is the total number of coincidences, μ is the attenuation coefficient and D is the thickness of the material the photons have to travel through. In PET/CT a comparison of the PET and the CT scan leads to an attenuation map of the patient due to their dependence on proton density in the material. Tissue with different attenuation coefficients is easily separable. To receive an attenuation map in PET/MRI is more challenging and a comparable result is currently not obtainable. At the moment there exist three different techniques to receive an attenuation map in PET/MRI. The segmentation-based and the atlas-based method rely on MRI, the emission-based method including emission only, joint-based and transmission-based (Tx-based) method, on PET.

The segmentation-based method separates MR images into different attenuating tissue classes. Problems of this method are the robustness of segmentation of tissue classes and the fast relaxation time T_2^* of bone. This leads to a nearly similar signal of air and bone in MRI, while in PET the attenuation coefficients of these tissues are on the different end of the scale (Tab. 2.1). Advantages of this method are the whole-body applicability as well as an easy implementation and low computational costs. By using a specific ultrashort echo time-based sequence, obtaining a signal from bone tissue in MRI was tried. As seen in Figure 2.4 the relative difference of PET/MRI to PET/CT is still in a range up to 20% for this method. [1, 3]

The second MRI based method is the atlas-based method. Here MRI images are combined with datasets with known attenuation coefficients derived from CT images. Due to local anatomic variants artifacts can appear in this method especially in whole body applications. Another disadvantage of this method is the computational cost. In contrast to the segmentation-based method, bone identification and continuous attenuation coefficients are given. Although it already improves the PET image, there are still differences compared with PET/CT. [1, 3]

The emission based method uses the emission PET data to calculate the linear attenuation coefficient. It can only give an approximation of the actual linear attenuation coefficient. [1]

The joint-based method uses iterative algorithms to estimate emission and attenuation. The disadvantage is that estimated emission and attenuation influence each other. Errors in the attenuation map compensate errors of the emission map. Also the high computational cost is a problem of the joint-based method. [1]

The Tx-based method requires an additional transmission source, which measures the attenuation at PET energy levels. Positive aspects are the whole body applicability as well as the robustness to artifacts. The transmission source exposes the patient with additional radiation but compared to PET/CT the dose is negligible. If transmission scans and emission scans are separated, the acquisition time is increased for this method. [1]

This project uses Tx-based method, but while it is currently only available by using the time of flight information, here the attenuation map is received by using an additional positron source in a liquid drive passing in a helical path around the patient. To obtain a suitable attenuation map for all tissues in the PET field of view the count rate at the detector is compared between a blank scan, where only the transmission source is inside the scanner, to a transmission scan with the patient in it. The difference in counts gives the attenuation for every line of response.

2.5 Fundamentals of fluid mechanics

This section will give the basic formulas needed to calculate the speed of the point source in the liquid drive. Fluid mechanical laws had a big influence on the choice of the pump as well as on the build up of the liquid drive. The velocity v depends on the volume flow rate Q and the flow cross chapter A .

2 Theory and background

T[°C]	$\nu[10^{-6} \text{ m}^2\text{s}^{-1}]$
20	1.004
21	0.980
22	0.956
23	0.934
24	0.912
25	0.891

Table 2.2: Kinematic viscosity ν of water at different temperatures T for a pressure of 1bar. The table is adapted to the room temperature in the laboratory.

$$v = \frac{Q}{A} = \frac{4Q}{d_i^2 \cdot \pi} \quad (2.8)$$

d_i is the inner diameter of the tube. According to the continuity equation, Q stays constant in the whole system. This means the velocity changes at junctions like the pump entry and exit or the additional devices to change the direction of flow.

With the aid of the velocity it also is possible to compute the Reynolds number Re to distinguish if the flow in the liquid drive is laminar or turbulent. Therefore also the dynamic viscosity η and the density ρ respectively the kinematic viscosity ν is needed.

$$Re = \frac{\rho \cdot v \cdot d_i}{\eta} = \frac{v \cdot d_i}{\nu} \quad (2.9)$$

If this dimensionless number is larger than 2300 turbulent flow is existent, a value below 1800 leads to laminar flow. Laminar flow means the fluid flows in fixed layers without influencing each other. In the transition zone between 1800 and 2300 first turbulences appear, above a Reynolds number of 2300 turbulent flow is given. [13]

The kinematic viscosity of a material depends on the temperature and on the pressure. While the influence of the pressure is negligible, the temperature has a severe effect on it. Table 2.2 lists some values around room temperature. The values are taken from [13]. As it is indirectly proportional to the Reynolds number and a temperature difference of only 5° leads already to changes of 10% of the kinematic viscosity, there is an additional influence on the whole system.

To receive the loss of pressure Δp in the system, it is possible to add the loss of every single component. On the one hand there is a loss because of friction in the tube which is calculated by

$$\Delta p = \frac{f \cdot L \cdot \rho \cdot v^2}{2d_i} \quad (2.10)$$

where f is the dimensionless Darcy friction coefficient, L is the length of the tube

2.5 Fundamentals of fluid mechanics

and ρ is the density of the flow material. While L and ρ are constants, f depends on the kind of flow given by the Reynolds number. For laminar flow it is calculated by

$$f = \frac{C}{Re} \quad (2.11)$$

with C as a constant depending on the sort of tube. For a circular one as the one used in this project C is given as:

$$C = 64 \quad (2.12)$$

For turbulent flow f must be computed iteratively and belongs on Re as well as on the pipe roughness ϵ

$$\frac{1}{\sqrt{f}} = -2 \log \left(\frac{\epsilon}{3.71 d_i} + \frac{2.51}{Re \cdot \sqrt{f}} \right) \quad (2.13)$$

ϵ depends on the material and is in the range of 0.0013mm and 0.0015mm for a new plastic. [14]

On the other hand a loss of pressure is given by the additional components in the liquid drive which can be estimated by

$$\Delta p_\zeta = \frac{\zeta \cdot \rho \cdot v^2}{2} \quad (2.14)$$

with the pressure loss coefficient ζ as a specific value for every component. For necking pieces those values depend on d_i of the tube as well as on d_i of the additional component. From the tight component to the broad component it is calculated by

$$\zeta = \left(1 - \left(\frac{d_{i1}}{d_{i2}} \right)^2 \right)^2 \quad (2.15)$$

where d_{i1} is always the diameter of the broader component [15]. In the other direction ζ can only be estimated because it belongs to the contraction coefficient α which can only be determined experimentally.

$$\zeta = \left(\frac{d_{i1}}{d_{i2}} \right)^4 \cdot \left(\frac{1}{\alpha} - 1 \right)^2 \quad (2.16)$$

Bending components rely on the angle and the relation of the inner diameter to the radius of the curvature. Additionally, it can depend on ϵ but because this value is very small for plastic, it is not considered in further calculations for these components. The only bending components needed in the liquid drive are 90°

2 Theory and background

curves which have

$$\zeta = 0.21 \quad (2.17)$$

because of a radius to diameter ratio of 1 and a neglectable ϵ . All the other curvatures especially the helical path of the tube around the PET/MRI head coil have no additional influence on the loss of pressure because the ratio of radius to tube diameter is too large [13].

2.6 Adaptive filter

The main aim of this master thesis is to develop a program to determine the position of the transmission source on its way through the liquid drive. To receive information for some spots Jones et al. [5] propose to use fiber optics at certain positions for this underpinning. To get a good estimation for the rest of the point source's path a program is necessary. The first idea was to use a Kalman filter which can predict a prospective position by combining receiving signals from the fiber optics with calculated predictions based on former signals. In this case, the Kalman filter can be reduced to one dimension only. For better notion it is like going in a tunnel with a car with a certain speed but losing the GPS signal. Information of the distance is provided by counting turns of the wheel but that is imprecise and additionally data is acquired by the speed sensor. A new mean μ_{new} is given by combining both measurements with their covariance σ to

$$\mu_{new} = \frac{\sigma_1 \cdot \mu_2 + \sigma_2 \cdot \mu_1}{\sigma_1 + \sigma_2} \quad (2.18)$$

and the covariance of the prediction is given by

$$\sigma_{new} = \frac{1}{\frac{1}{\sigma_1} + \frac{1}{\sigma_2}} \quad (2.19)$$

In the particular case of this project μ_1 is the position of the measurement and σ_1 the corresponding covariance, while μ_2 the position calculated from the velocity again with its covariance σ_2 . A perfect measurement means a noise of 0 and according to that one of the covariances σ becomes 0 as well. In further implementation this leads to a very small σ_1 due to quite exact localizing with the fiber optics and a larger σ_2 because the velocity is more imprecise. Accuracy decreases while the prediction step and increases when the measurement is updated. If the prediction has been good the covariance becomes smaller and total accuracy is better. [16]

Although the Kalman filter can predict the position quite accurate, a new idea came up regarding the actual velocity between the positions and the movement within a 360° turn. While the Kalman filter is predicting future positions, in this program the point source is located afterwards. The disadvantage is that there is no live tracking available for this method. On the other hand localization of the pellet can happen subsequently because evaluation of PET data takes time too. As it uses always the real velocity between two positions it is more precise than predicting the velocity. A detailed description how the positioning happens, is given in Section 3.4.

2.7 PET/MRI head coil

The PET/MRI head coil is as a receiving coil developed and built by the RF Lab at the MR Center of Excellence. All the following details are given by [6]. While the used PET/MRI is MRI based, this device can be used for Tx-based attenuation correction. Additionally, it is a much more sensitive receiving coil than the one implemented in the PET/MRI itself because it is very close to the examination area. In contrast to the PET/MRI which can be used for whole body scans, the field of applications is specialized to head and brain studies for this coil.

The housing consists of an inner and an outer shell, 3D-printed from laser-sintered polyaurinlactam. The inner shell (Fig. 2.6 right) is elliptical and contains the RF coil array. The structure of the coil layout is chosen in a way that the desired penetration depth (~ 10 cm) of MRI is given, as well as geometrical concerns like head and neck coverage and space for shoulders are considered. In addition strongly PET signal attenuating components, especially preamplifier, are placed outside the PET field of view (FOV), which is smaller than the MRI FOV (Fig. 2.5). 24 coil elements in 4 rows (7+7+7+3) are merged to 3 coil plugs with 8 channels each. Within the rows transformer decoupling is given (marked orange in Fig. 2.5). The outer shell (Fig. 2.6 left) serves as a cover for the RF-coil array and base for the hydraulic drive. It is cylindrical and its thickness is minimized to 4 mm to reduce attenuation. The diameter of the outer shell is 32 cm, which leads to a length of 100,53 cm per 360° turn. The hose circles the outer shell 20 times resulting in a length of approximately 20 m. 4 bars from the front to the back fix the hose to provide consistent turns for the transmission source. The bars are marked from A-D, starting at the top and proceeding counter-clockwise. The D-bar is visible in Figure 2.6. Small holes in the bars allow to fix the fiber optic cable on the PET/MRI head coil. On the inner side is a sliding guide to enable

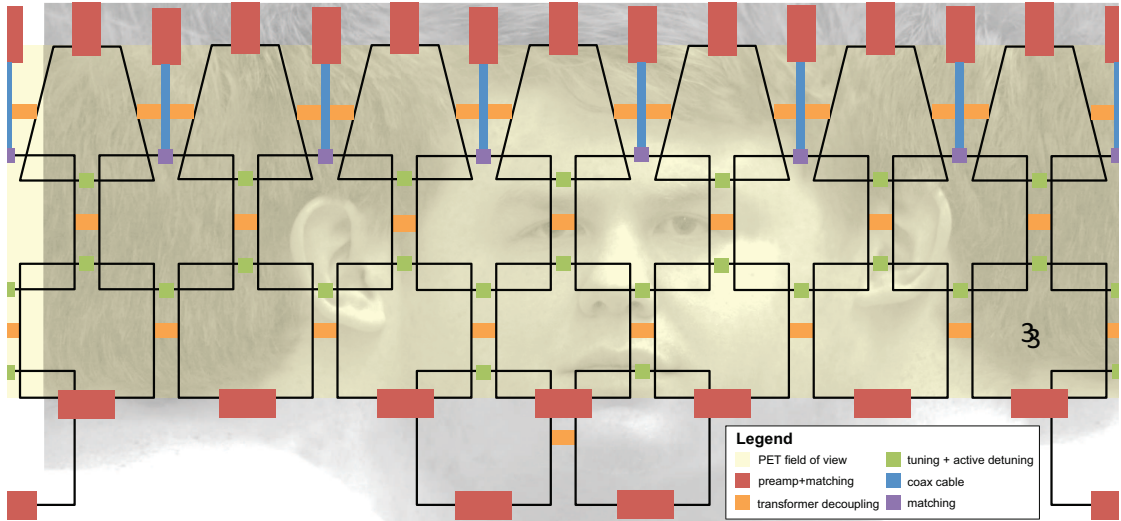


Figure 2.5: Coil element layout of the PET/MRI head coil. MRI-FOV is larger than PET-FOV (light-green). Components with high attenuation in PET (red) are outside PET-FOV. The bottom row has only 3 elements to cover the neck in MRI-FOV but also provides space for shoulders [6].

easy integration and removal of the inner shell. More details will be explained in Section 3.1.3.

2.8 Lightbarrier

The lightbarrier system is the external tracking system of the transmission source. The general setup how it identifies the pellet is shown in Figure 2.7. A light emitting diode (LED) acts as light source inducing an optical signal at the photodiode. This signal is converted to an electrical signal and amplified afterwards. The received signal is compared to a threshold, which depends on the light intensity. The system contains 16 independent light barriers and amplifiers. The information is collected in form of a timestamp and the position of the trigger and is collected by a micro-controller. The device is connected via USB with the PC (Fig. 2.8). The user receives the information by a graphical user interface (GUI). [8]

A MRI compatible polymer optical fiber delivers the light of the LED to the desired position of the PET/MRI head coil and another one receives the signal. In total 81 pairs of holes are drilled into the bars from the back to the front, 21 at the bottom bar and 20 each at the others allowing different possibilities of localization of the transmission source. They have a diameter of 2.2 mm which is similar to the diameter of the fibers to receive a fixed connection by sticking the fibers in.

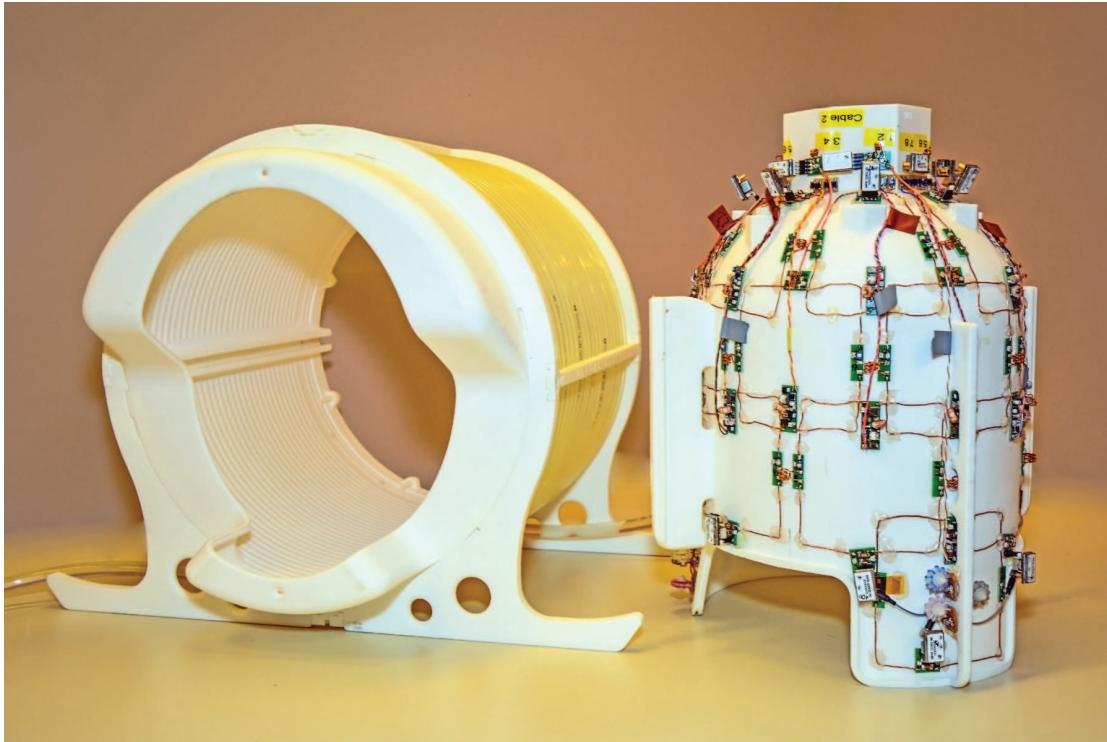


Figure 2.6: Outer shell with hose system (left) and inner shell (right) of the prototype of the PET/MRI head coil [6].

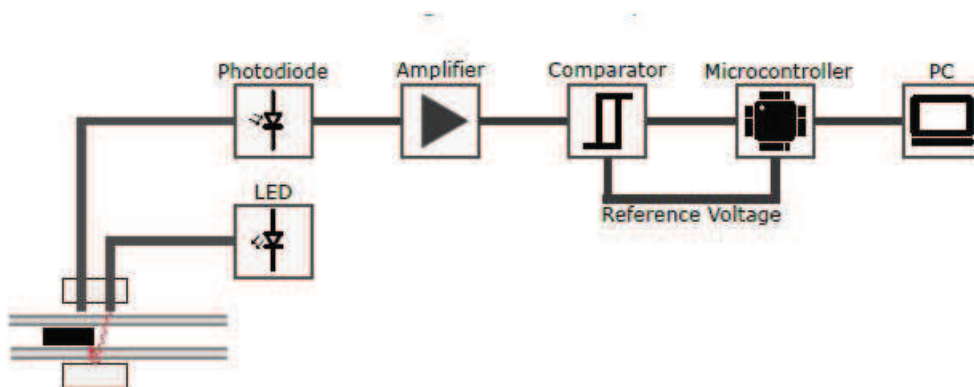


Figure 2.7: Lightbarrier block diagram: A LED sends light to the desired position and when the pellet passes by the light intensity at the photo-diode changes. This signal is amplified and compared versus a threshold. A micro-controller collects the information and sends it to the PC [8].

2 Theory and background

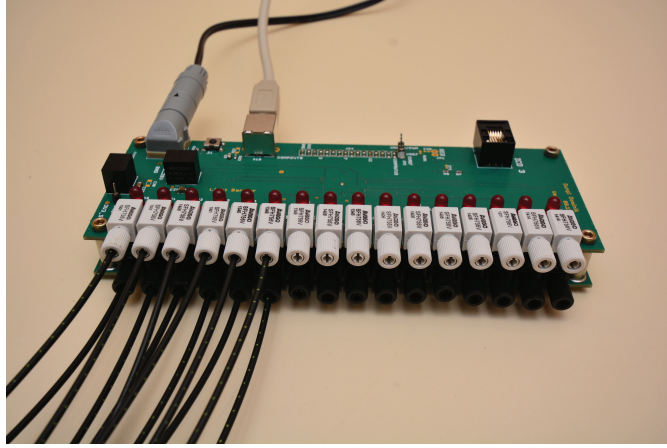


Figure 2.8: Lightbarrier tool with fiber cables. LEDs in the top row provide light to the desired position, the bottom row is receiving the signal if the pellet passes by, turning on the red indicator LEDs. In the back the power supply connection (left cable) and the USB connection (right cable) can be seen [8].

Different possibilities of hole arrangement were tested, resulting in two parallel holes close together as best solution for signal tracking with the fiber optics. At the tracking position the light transmits through the hose and is reflected diffusely by white plastic of the PET/MRI head coil and travels back to the second fiber, which delivers the signal to the photo-diode. When the pellet passes by, the light is blocked and an optical signal is induced. The intensity at the photo-diode decreases as soon as the pellet blocks the light and increases after the pellet has left the measuring position. Both events are registered and display a signal. [8]

The threshold is chosen in a way that artifacts from air bubbles should not induce signals at the lightbarrier device. This means that only the transmission source should lead to an registered event. Furthermore signals from the adjacent positions are eliminated by the threshold. Additionally, the attenuation loss of the fiber must be taken into account.

$$a = 10 \log \left(\frac{P_1}{P_2} \right) \quad (2.20)$$

The attenuation a belongs to the length l of the fiber and the attenuation factor α which is a specific constant.

$$a = l \cdot \alpha \quad (2.21)$$

P_1 is the incoming power and P_2 the power at the end of the fiber. As either P_1 nor P_2 are measured only the ratio can be calculated. Some transformations lead to

$$P_2 = \frac{1}{10^{\frac{\alpha}{10}}} \cdot P_1 \quad (2.22)$$

According to the data-sheet α is $0.15 \frac{dB}{m}$ at the used wavelength of 650 nm [17]. As the fibers have a length of approximately 7 m, the attenuation of light intensity is about 1 dB. Inserting the data in Equation 2.22 the intensity loss is more than 20% for each of the fibers. Reducing the length of the fiber is not possible because the device itself contains metal elements and is therefore not compatible with MRI. This means the device is placed in the control room outside of the PET/MRI.

In addition, attenuation occurs by bending the fiber cables. Especially for the position at the bottom bar the maximum bending radius of 9 mm is used. Measurements led to a further reduction to the half intensity compared to totally stretched fibers. Nevertheless it is still possible to detect the pellet at every position.

The GUI used is an improved version of the interface developed in [8]. In the original version it has been possible to receive timestamps of the lightbarrier system when the pellet has passed a cable position. The number has been given in μs beginning with the moment the device has been plugged in. After 4295 s, which is approximately $2^{32} \mu s$, the received timestamps have started again at 0. The number is defined by the maximum size of the unsigned double value. The received timestamps have been able to be saved in a .csv file as well as in a .txt file.

2.9 Qt

The cross-platform application Qt, short for ‘cute’, is a C++ based application developing software. Furthermore additional Qt libraries exist as well as the Qt-Creator. It is supported by different platforms and used in many companies in medical, automotive or infotainment technologies. [18]

2.9.1 Qt Designer

With aid of the Qt Designer GUIs with Qt Widgets can be designed and built. The properties of code changes dynamically by implementing forms and widgets. It uses the Qt’s signal and slots mechanism which allows to integrate the widgets and forms easily with the programmed code. [19]

This mechanism is responsible for the communication between objects. When one signal is induced, for example by clicking a button, a particular response occurs. An objects emits a signal which leads to the execution of the linked

2 Theory and background

slots immediately. This happens as in a normal function and is not influenced by any GUI event loop. One signal can induce several slots which are executed subsequently. Slots are C++ functions following the C++ rules. [20]

2.9.2 Qt-Creator

The cross-platform integrated development environment (IDE) of Qt is the Qt Creator. It is the tool to create mobile apps as well desktop applications and connected embedded devices. The main target is to simplify application and UI development. [21]

3 Materials and methods

This chapter deals with the equipment used in this project. It will explain technical details about the liquid drive and the pellet. Additionally, the software of the lightbarrier system will be described and also details of the code used in the filter are explained in this chapter.

3.1 Liquid drive

The liquid drive consists of three parts. A voltage source provides the power for a pump which is part of the hydraulic drive. From there, water is driven through the tube system, which contains the hose itself as well as the direction control and the compensating reservoir to inject and remove the pellet.

3.1.1 Voltage source

The used power supply to move the pellet through the tube system is the Weir 4000 (Fig. 3.1). This device has 2 independent outputs which have a working range of 0-30 V voltage and 0-2 A current. It is possible to regulate voltage as well as current separately by turning the corresponding knob. The upper knobs control the voltage output. For rough adjustment the right one is needed, fine adaption is controlled by the left knob. In this project mainly the upper right one was used which means regulation was voltage controlled. Current regulation, done by turning the knob in the lower section next to the *A*, leads to jumps in voltage and according to that to changes in velocity. Therefore the knob for current adjustment was fixed in maximum position. Accuracy given with the knob for rough voltage control is about 0.1 V but voltage decreases up to 0.03 V for small and 0.3 V for high voltages within some time.

Due to inhomogeneities of around 1.5 % in voltage output, time varies even for the same voltage. Additionally, the velocity changes within a scan. Dispersion is larger for small voltage because there changes have a bigger influence on the velocity (see Chapter 4.1).

3 Materials and methods

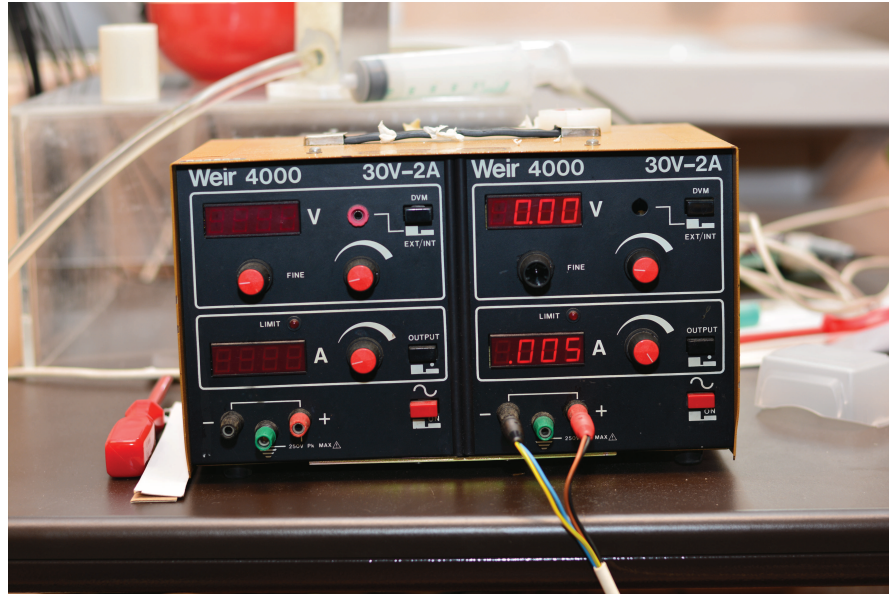


Figure 3.1: Weir 4000 power supply: Two different outputs (right and left) with a working range of up to 30 V and 2 A. Adjustment is done by turning the knobs. The upper row regulates the voltage, the lower row the current.

3.1.2 Pump

The motor driving the pellet through the liquid drive is the BP-50 Bio Pump, a Centrifugal Blood Pump of the Medtronic, Inc. Corp. (Fig. 3.2). The original purpose of this pump is to maintain the blood circulation during cardiac surgery. It has an inlet and outlet port of 1/4 inches, which is 6.35 mm and an inner volume of 48 ml. The size of the ports can be easily connected to the used hose with an inner diameter of 8 mm. The maximum flow rate is 1.5 l/min [22].

The choice of the pump perfectly reflects the requirements of a small inner volume



Figure 3.2: BP-50 Bio Pump

and a flow rate of around 1 l/min. The only disadvantage is the restriction to one way which leads to an additional direction control, a part of the tube system explained in Section 3.1.3. The inner volume should be small because of the price of heavy water which will be used in the final version. The whole system contains approximately 1.6 l, therefore it is possible to pump nearly the whole content within one minute through the system. This means a change of water, which is needed from time to time to get rid of dust particles which enter the liquid drive via the compensating reservoir can be done within several minutes.

The helical path around the PET/MRI head coil, which is approximately 2/3 of the whole liquid drive, can be passed in approximately 40 s with this pump but at these high velocities air bubbles can appear in the liquid drive. If those air bubbles arrive at the pump they stay inside until it is turned off. By moving the pump they can be removed to the outlet port from where they are driven to the compensating reservoir and there they vanish again.

3.1.3 Tube system

The tube system is the main part of this project. Main requirements were an easy handling of the pellet and the possibility of a change in direction without additional handling to avoid radiation. Furthermore the transmission source is not allowed to leave the PET/MRI room but either the power supply nor the pump were allowed to be placed inside that room due to their incompatibility with the MRI. Stability as well as maintainability were also demanded. Other important aspects were the easy injection and removal of the pellet in the tube system and the minimization of water loss.

The selected hose has an inner diameter of 8 mm and an outer diameter of 12 mm. It is transparent polyurethane tube to allow detection of the pellet with the lightbarrier system. During test phase the filling is distilled water, the final version will contain heavy water because of its invisibility in MRI. The system consists of three main parts:

- the one which has to be inside the PET/MRI room where the transmission source is moving
- the connection between the PET/MRI room and the control room and
- the part in the control room where the distinction of direction takes place.

The first part is by far the longest with a length of around 26 m. It includes the compensating reservoir, the tube with the helical path around the PET/MRI head

3 Materials and methods

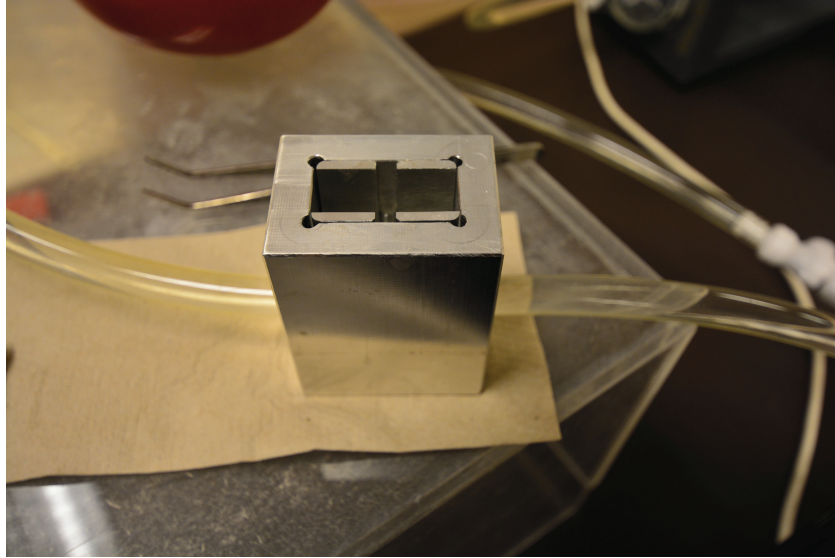


Figure 3.3: Compensating reservoir connected to the hose. The metal part in the middle is removable and deals as sliding guide.

coil and a necking piece at each end of this part. The compensating reservoir (Fig. 3.3) is a 4 cm x 5.5 cm x 7 cm aluminum box which is open on the top. Additionally, there exist holes in the side walls with an diameter of 12 mm to provide an easy connection to the hose. For the safe input of the pellet, a removable sliding guide is placed inside the box. To support fast removing 2 slits in the middle of the sliding guide for forceps are given. As it is the only open part, it has to be placed at the highest position in the system to avoid the loss of water due to the hydrostatic pressure. At this spot also evaporation over time is visible. The amount of lost water is discussed in Section 4.6.

Starting at the compensating reservoir, the transmission source travels about 2.5 m to reach the first of 20 rounds at the PET/MRI head coil. Each round has a length of 100,53 cm resulting in a total length of 20,1 m for the pellet around the patient. In this section the hose is arranged in a helical way. Afterwards there are again 3 m of hose leading the radioactive source away from the patient to the second necking piece to stop the pellet.

Beside stopping the pellet inside the PET/MRI room, these necking pieces (Fig. (3.4)) provide the possibility of disconnecting the first part, where the pellet moves, from the others. This is useful especially in transporting the whole device but must be done carefully to prevent dropping of water. After sticking the parts together air stays in the connecting piece which can be eliminated by turning on a high voltage and bringing the air bubble back to the compensating reservoir.

The second part is the connecting part between the PET/MRI room and the control room. A tunnel in the wall allows to lead the hose and the bundle of fiber

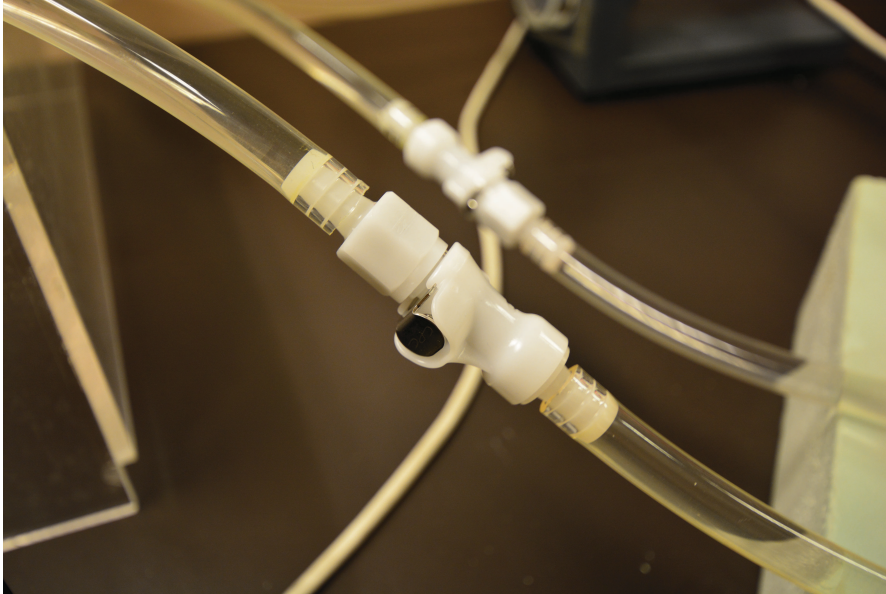


Figure 3.4: Connecting pieces which act as stoppers of the transmission source on the one hand side and as possibility to disconnect the first part of the liquid drive from the others on the other hand.

optics out. This section of the tube has two times a length of 2,5 m and ends at the direction controlling tool. It consists only of the hose.

The third part of the tube system is the part in the control room. It consists of the pump followed by 40 cm of hose and the direction control. The first arrangement tested (Fig. 3.5a) looked like the literal “4”. It fulfilled the main purpose of smooth direction change by turning the three-way valves. The disadvantage of this system was the different path-length as well as different total resistance due to an additional curve for the different directions. In the final configuration (Fig. 3.5b) the curve was eliminated which leads to the same path for both directions. If the pellet has to move from the compensating reservoir to the PET/MRI head coil the three-way valves have the configuration as in the figure, for the other direction the way between valve 1 and 2 and valve 3 and 4 is closed. The advantage of the second arrangement is that both directions have the exact same way which leads to the same loss of pressure for both directions.

To exchange the water in the system the hose is disconnected from the compensating reservoir and the direction control is set in backwards direction, which is the 2nd arrangement mentioned above. An air bubble enters the end of the hose and afterwards the hose is connected to a fresh water reservoir. Now the pump is turned on leading the air bubble to it. When it arrives there the voltage source is turned off again and air is removed from the pump and voltage is applied again. Fresh water is aspirated and the old water is pressed out on the other end of the hose. When the air bubble arrives at the end the exchange of water is performed.

3 Materials and methods

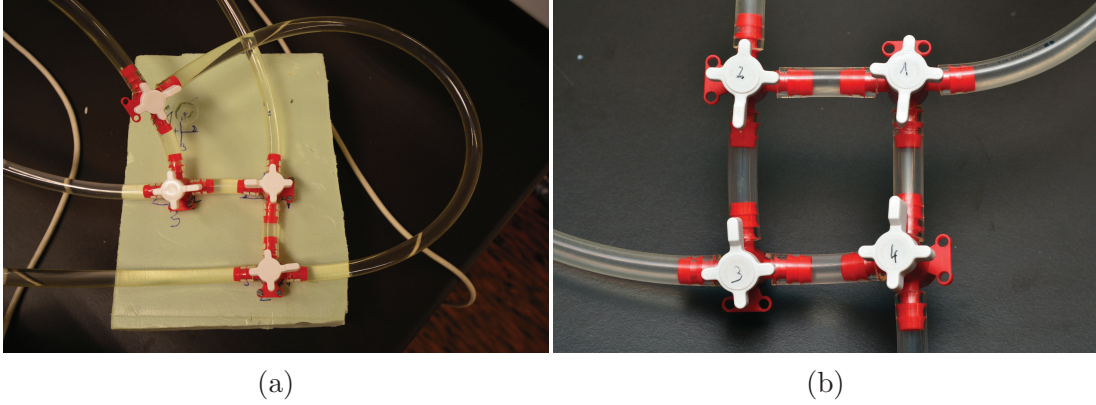


Figure 3.5: On the left side the first arrangement of the direction control is visible. The total distance is slightly different and additional resistance due to the curve is given. In the final arrangement in the right picture these factors are eliminated.

Table 3.1 shows all used components within the liquid drive. The second column gives the number how often this element is present. The curvatures represent the 90°-arches of the direction control. Additionally, the three way valves are responsible for 4 of 8 necking piece entrances and exits. The stoppers are 2 further necking pieces. The 7th necking position exists short before the entrance of the pump because the hose has to be sticked to the pump and therefore an additional necking piece is at the exit behind the pump. The last necking element was mainly used in the beginning of the project where the compensating reservoir has not been available and elimination of air was hardly possible. This has been done by an additional component. All this previous elements reduce the diameter at the entrance from 8 mm to 6 mm and raise it again to 8 mm at the exit.

At the entrance and exit of the compensating reservoir a change from 8 mm to 10 mm is assumed as the sliding guides stick quite close to the holes for the tube and with appropriate filling of the compensating reservoir just a small gap is necessary. The biggest change in diameter exists at the pump where it raises from 6 mm to the pump diameter of 90 mm, but because the pump is seen as a black-box in closed systems this components have no influence on the loss of pressure.

The third column gives the calculated pressure loss coefficients. The values are calculated by using the Equations 2.15 and 2.16. The values for α determined in Equation 2.16 are listed in Table 3.2. As explained these values rely on experimental data and are taken from [13]. ζ always represents the value at the incoming diameter. As seen in Table 3.1 the by far highest value is given at the pump exit. Therefore according to continuity equation the resulting velocity is the lowest which means that the pressure loss is not that high (see Sect. 4.2).

Component	n	ζ
Necking pieces entrance	8	0.191
Necking piece exit	8	0.691
Compensating reservoir entrance	1	0.130
Compensating reservoir exit	1	0.439
Pump entrance	1	0.991
Pump exit	1	25192
Curvatures in direction control	2	0.210

Table 3.1: Components of the liquid drive. The second column gives the number n how often the component is used in the liquid drive and the last column the pressure loss coefficient ζ .

Component	α
Necking piece exit	0.681
Compensating reservoir exit	0.586
Pump exit	0.702

Table 3.2: α -values of components where the diameter decreases.

3.2 Pellet

In this section the transmission source is explained. The main requirements are the safe transport of the radioactive source, a sufficient activity which allows the determination of the attenuation coefficients and additionally the localization of the source should be possible at every moment of the path through the liquid drive. Furthermore the movement should be consistent and of course the material used must be MRI compatible.

Considering the tube diameter and the maximum bending in the liquid drive, calculations led to a maximum length of approximately 29 mm at a diameter of approximately 7 mm. Table 3.3 shows the most important parameter of the different planned pellets. The first prototype of the pellet has been a duroplastic with a length of 28,25 mm, a diameter of 7,25 mm and an inner height of 12.75 mm. It is possible to go through the whole system with this pellet. Starting from this, it was possible to construct other pellets out of different materials. Calculations have been done for aluminum, PMMA and titanium.

As all of these materials have a higher density than water; Floating of the pellet is achieved by a combination of the radioactive solution and air in the pellet. Furthermore the screw to fix the content in the pellet must be regarded. Here, the decision fell on a 9.25 mm plastic screw with a density of nylan (see Tab. 3.5). The head of the screw is reduced to the minimum that it has the same diameter as the screw itself. The length of the screw has also an influence on the inner height

3 Materials and methods

Pellet	l [mm]	d [mm]	Wall thickness [mm]	Inner height [mm]
Prototype	28.25	7.25	0.75	12.75
PMMA	24	7.4	0.75	15
Aluminium	24	7.4	0.3	16
Titan	24	7.4	0.2	16.6

Table 3.3: Parameters which are taken into account for the pellet choice. Length l and diameter d must consider the diameter of the tube and the radius of the PET/MRI head-coil. The inner height is the result of length minus bottom strength and screw length.

Pellet	V [μ l]	V _{H₂O} [μ l]	V _{D₂O} [μ l]
Prototype	331	50	-
PMMA	410	293	392
Aluminium	581	201	310
Titanium	638	160	269

Table 3.4: Resulting volumes for the pellets described in Table 3.3. In the second column shows the total available volume V , beside it the perfect filling volume V_{H_2O} for floating in the testing phase with distilled water and in the last column the perfect filling volume V_{D_2O} for floating in the final state with heavy water in the liquid drive are present.

of all pellets. The rest missing on the total length is the thickness of the bottom. Different wall and bottom thicknesses lead to different available volumes, shown in the second column of Table 3.4.

The perfect filling for floating depends on the density of the pellet material. As seen in Table 3.4 the aluminum pellet and the titanium pellet have much higher available volumes but floating is achieved with a lower volume than in the PMMA pellet. Furthermore this filling volume is only available by using a polyethylene plug between the screw and the material.

The reason why these volumes are of importance is the consistency of movement within a round. A pellet with a density below the density of the surrounding material will accelerate while ascending in the tube around the PET/MRI head coil and a heavy pellet will do the same while descending (see Sect. 4.3). According to Table 3.4, the decision has been to produce a PMMA pellet and an aluminum pellet as a higher floating volume means more solution can be filled in and a higher count rate for the PET/MRI is possible.

To achieve a perfect filling a 5 ml syringe is used. This results in an accuracy of approximately 20 μ l for the volume inside the pellet. An ideally filled pellet is shown in Figure 3.6. In this picture the different sections are visible. Beside the solution, air resides inside. As air has a lower density than the solution the bubble always moves to the top position. This means while ascending it is located below

Material	Density [g/cm ³]
PMMA [23]	1.18
Aluminium [23]	2.7
Titanium	4.507
Plastic screw	1.6
Polyethylene [23]	0.925
Water	1
Heavy water	1.106
Filling solution	1.005
Air	0.0012

Table 3.5: Densities of materials used for volume calculations of the pellet.



Figure 3.6: Perfectly filled PMMA pellet in the testing phase. The total length of 24 mm is separated in 2 mm bottom, 10.6 mm of the solution and 4.4 mm of air. Above the screw with a total length of 9.25 mm, 7 mm inside the pellet and 2.25 mm outside are visible.

the screw as seen in Figure 3.6 while the bubble travels within the pellet to the other side while descending. This leads to an additional torsional moment (see Sect. 4.4).

All these facts above support the PMMA pellet as best choice for this project. It has the highest possible floating volume, does not need a polyethylene plug, which means that it has the same material density at both ends and additionally the air volume is small in comparison to the other types. In the final version with heavy water inside the liquid drive, it should be nearly full which will mean that it is balanced and has no torsional moment at all while floating.

A big disadvantage of the PMMA pellet is its transparency. This means it is hardly detectable by the lightbarrier system. This is the reason why it is colored black with a water resistant marker. Additionally, the shape with the sharp end at the

3 Materials and methods

top of the pellet is not perfectly fitting with the lightbarrier which leads to the use of only one timestamp per cable position of the lightbarrier.

The other pellets were mainly constructed because of their high inner volume which possibly leads to a higher count rate of the PET/MRI. Results of experiments in the PET/MRI have shown that the volume of the PMMA pellet induce a high enough count rate and the other advantages of the PMMA pellet predominate the aluminum and titanium pellet. Therefore, in further sections by the term pellet always the PMMA pellet is meant.

3.3 Lightbarrier system

The GUI used is an improved version of the original developed by [8]. Features which have been implemented within this thesis are the “Cable Position” window, the “Initial Parameters” window as well as the time synchronization between the computer and the lightbarrier system. Furthermore the data saved has been changed.

In a first task, time synchronization with the computer has been arranged. At the moment the signal arrives at the computer beside the lightbarrier system time, the computer time in ms since start of system clock is visible. The second and third column always show the last registered timestamp of the cable position. In the beginning of the measurement it says “nothing detected yet” by receiving a signal this changes into the number of μs for the lightbarrier system time respectively the number of ms for the computer time. If after a whole trip of the transmission source the phrase is still placed in the slot instead of a number, this means that this cable pair has failed in detecting the pellet while passing by. Due to hypersensitivity of the lightbarrier system, it can also happen that more than 2 timestamps are recognized. This leads to an overloaded buffer which results a delayed output of the lightbarrier system. While the time of the lightbarrier system is stored in the buffer in this case the synchronized time is belated. To avoid mistakes, calculations always use the time differences of the lightbarrier system and convert them into the computer time in ms. Furthermore, if a future position has a smaller timestamp than the one before, the number of ms can be added to prevent failures from the maximum time of the lightbarrier system signal. This is essential for calculating the velocity and exact position later on.

The “Cable Positions” window deals with the arrangement of the cables at the PET/MRI head coil. As explained in Section 2.7 81 pairs of holes are drilled into the 4 bars from the front to the back. This dialog assigns which pair of holes

3.3 Lightbarrier system

is used to have the possibility to compute the velocity within two neighboring positions. While the arrangement of the light conductors can be random, the signal receiving cables should be in ascending order from the back to the front of the head coil system, which means ascending in the frontwards direction of the liquid drive. This means the first signal is received by position 0 followed by position 1 and further on. The first column in the window gives the round number the cable is stucked to with available numbers between 1 and 21. The second column determines the position within the round. 0 means hereby the bottom position (C-bar), 1 is the position after 90° (B-bar), 2 the top bar (A-bar) and 3 the position after 270° (D-bar). The adjusted parameters contain the first position where the tracking starts as well as the last position (Position 0 has as start of the first round 1 0 as parameters, Position 15 has 21 0 as it is the 21st bottom position) and two complete rounds with cables at five consecutive positions to determine the difference of velocity in the 90°-segments. The remaining four cables are placed at the top bar in approximately equal distances to each other. Changes of the initial arrangement can be stored in this dialog of the GUI.

As initial parameters the voltage, the direction and the end of the pellet are respected. These parameters also find use in the calculations afterwards. The voltage slicer has a range of 1.8 V to 12 V. For this slicer a rough estimation of the value is enough, it is only responsible for a rough velocity estimation. The other boxes are far more important. The flow direction is self-explanatory. It determines the start of the calculations of the filter. The third box considers the end of the pellet. As both ends have different shapes, detection can happen at different parts of the transmission source. The flat end is more consistent than the pointed end and therefore it is the one which is taken into account for determination when the pellet passes by. If the flat end is in front the first timestamp of each position is considered, while if it is in the back the last timestamp defines the position.

The last change of the software is related to the output in the .csv file. While in the beginning the file contained only the positions with their timestamps, the present file starts with the parameters given in the “Initial Parameters” window and the total time needed in ms. In the next lines timestamps for every calculated position are shown. The step size is approximately 0.1° which means for 20 full rounds the system returns 72000 positions with their calculated timestamps. As one round has a length of 100.53 cm the step size is approximately

$$\frac{100.53 \text{ cm}}{3600^\circ} \approx 0.028 \text{ cm} \quad (3.1)$$

The way how the positions are computed is given in Section 3.4. In the end of the file also other relevant parameters for the calculations can be found. Hereby, the

Code segment 3.1: Code segment which shows how unnecessary data for the thin end in front is deleted.

```
for (int i=0; i < DetectionData.size()-3; i+=3)
{
    if (DetectionData [ i+3]==DetectionData [ i ])
    {
        continue;
    }
    else
    {
        PosTime.append ( DetectionData [ i ] );
        PosTime.append ( DetectionData [ i +1 ] );
        PosTime.append ( DetectionData [ i +2 ] );
    }
}
```

velocity between two neighboring positions as well as the correction factors for the different quarters are visible. Additionally, the adjusted cable positions from the “Cable Positions” window are present.

3.4 Program and Filter

The filter used for position determination considers the velocity between two neighboring positions as well as the correction factors for the different quarters.

In a first class all the unnecessary data is deleted to receive only one timestamp per position. By comparing the registered positions, equal positions are sorted out. Code segment 3.1 shows how this works for the thin pellet frontwards. This implements that always the last timestamp of the position is used for calculations. If the registered position is now equal to the one next one, it is omitted. If the next position is different, it is the last timestamp of the position which leads to the attachment of the position, its lightbarrier timestamp and the computer time to the `PosTime` vector.

If the thick end arrives first at the cable position, the first timestamp of each position is taken. Therefore only the 3rd line changes to code segment 3.2. All the other timestamps of the `DetectionData` vector are dismissed and only the `PosTime` vector is used for further calculations. The `DetectionData` vector always contains a position as the first element, a timestamp of the lightbarrier system as a second element and the corresponding computer time as a third element. This order repeats until the end of the vector. Therefore 3 elements are handed to the

Code segment 3.2: Changes if the thick end is in front. Here the first timestamp of each position is needed.

```
if (DetectionData [ i]==DetectionData [ i -3])
```

Code segment 3.3: Time correction if later timestamp has a lower number than the one before.

```
for (int i=1; i<PosTime.size () -3; i+=3)
{
    if (PosTime [ i]>PosTime [ i +3])
    {
        PosTime [ i +3]=PosTime [ i +3]+429496729;
    }
}
```

`PosTime` vector and because only the positions are compared with each other only every 3rd element is checked.

Another important function in this class is code segment 3.3. As explained in Section 3.3 the lightbarrier system only counts up to approximately 4295s and starts again with 0 afterwards. This code segment compares the received timestamps in the `PosTime` vector. Therefore all lightbarrier timestamps are divided by 10 and if the lightbarrier time of a later segment is lower than of the one before, it is corrected by adding the factor

$$429496729 \approx \frac{2^{32}}{10} \quad (3.2)$$

As this function matches the lightbarrier system timestamps, it starts with the second element of the `PosTime` vector.

The corrected elements of the `PosTime` vector are the base for the calculation class. Instead of a Kalman filter which estimates the actual velocity on base of former velocities, in this program the velocity is calculated afterwards. The main factors therefore are the velocity between two positions and the quarter coefficients which are the multiplying factor and depend on the position within one round.

These correction factors are computed first. The elements of the `cabpos` vector, which contains the registered cable positions, are checked against each other to find complete rounds with 5 consecutive cable positions. If there is a complete round available the time difference between these two positions is determined and is given to the `roundTime` vector. Additionally, this vector receives the cable position of the start as well as the cable position of the end of the round (upper

Code segment 3.4: Determination of quarter coefficients

```

for (int i=0; i<cabpos.size(); i++)
{
    for (int j=i+1; j<cabpos.size(); j++)
    {
        if (cabpos[j]-cabpos[i]==36000)
        {
            roundtime= PosTime[3*j+1]-PosTime[3*i+1];
            roundTime.append(roundtime);
            roundTime.append(cabpos[i]);
            roundTime.append(cabpos[j]);
        }
        if (cabpos[j]-cabpos[i]==9000)
        {
            if (cabpos[j]%36000==9000 && cabpos[i]%36000==0)
            {
                quarterTime = PosTime[3*j+1]-PosTime[3*i+1];
                quarter1Time.append(quarterTime);
                quarter1Time.append(cabpos[i]);
                quarter1Time.append(cabpos[j]);
            }
            ...
        }
    }
}

```

section of code segment 3.4).

In a next step also the quarters are identified. Therefore the `cabpos` vector is checked for positions with 90° difference and if it is available, it is identified which quarter is on hand by using the modulo operator. The multiplication factor of 100 guarantees a better accuracy for the position variable later on. In the lower section of code segment 3.4 the calculation for the first quarter in frontwards direction is visible. In total there are 4 vectors, one for each quarter.

To receive the correction factors for every position, the quarter times are divided through the round-times afterwards. In the best case every position is detected twice, which implements 2 quarter coefficients for every segment. As they are time depending and velocity is indirectly proportional to the time, the velocity correction factors are computed by dividing 1 through the mean of quarter coefficient for every segment. These factors are called `quartercoeff1-4` in the end. Additionally, a `Velocity` vector is generated which contains the velocities between two neighboring positions.

In the next step the actual position determines the actual velocity. The position

Code segment 3.5: Determination of actual velocity

```

if(pos > cabpos[1] && pos < cabpos[2])
{
    if(pos%36000<9000)
    {
        velo = Velocity[1]*quartercoeff1;
    }
    if(pos%36000 > 8999 && pos%36000 < 18000)
    {
        velo = Velocity[1]*quartercoeff2;
    }
    if(pos%36000 > 17999 && pos%36000 < 27000)
    {
        velo = Velocity[1]*quartercoeff3;
    }
    if(pos%36000 > 26999)
    {
        velo = Velocity[1]*quartercoeff4;
    }
}

```

Code segment 3.6: Velocity reset for successive positions

```

for(int i=0; i<cabpos.size()-1; i++)
{
    if(cabpos[i+1]-cabpos[i]==9000 && pos > cabpos[i]
        && pos < cabpos[i+1])
    {
        velo = Velocity[i];
    }
}

```

is checked against the elements of the `cabpos` vector to know which velocity is relevant for it. Afterwards the position within the round is identified by the modulo operator and the corresponding quarter coefficient is multiplied with the actual velocity. Code segment 3.5 shows an example for frontwards movement between the second and the third detected position.

For successive cable positions it is not necessary to correct the velocity as it is more accurate by using its own speed. Therefore code segment 3.6 is implemented in the program. If the difference between two positions is 90° and the actual position is between these `cabpos` positions, the velocity is reseted to the uncorrected value of the `Velocity` vector.

Finally the velocity is multiplied with the `timeStep`, which is defined by the time

3 Materials and methods

Code segment 3.7: Determination of the new position with its time at the computer and the lightbarrier system.

```
actpos = actpos + velo * timeStep;  
actcomptime = PosTime[2]+i*timeStep;  
actsystime = PosTime[1]+i*timeStepSys;
```

difference between the first and the last position divided by the difference of the first and the last position in hundredth of degrees. By adding this product to the position a new actual position is determined and the whole circle between code segment 3.5 and 3.7 starts again.

Additionally to the actual position, time marks are calculated in each step. The `actcomptime` variable generates a timestamp in ms since start of the day while the variable `actsystime` determines the value of the lightbarrier system in μs to have the possibility to compare registered timestamps with the calculated version. All the variables in code segment 3.7 are assigned to vectors after each circle in the *for*-loop.

By pressing the “Save” button after the pellet passed through the system the classes described before are executed. In the first lines the initial parameters are written followed by the total time needed to pass through the system. The main part of the .csv sheet is the part with the position in degrees with its corresponding timestamps both of the computer time and the lightbarrier system. Below this section all important parameters used to determine these positions are also given.

4 Results and Discussion

This chapter deals with the details of the different measurements performed during the testing phase. The first section explains how flow rate, velocity and the voltage of the power source are linked to each other. The following section will describe the loss of pressure appearing in the liquid drive for selected flow rates.

Afterwards it will be explained how the filling of the pellet influences the movement. It will show within which range the filling must stay to ensure more or less consistent travel. Further sections will deal with the consistency of round times for different voltages and the movement within one round. The loss of water in the liquid drive will be also discussed shortly.

The last section will explain how the lightbarrier system should be used and which preparations must be taken into account to ensure proper results.

4.1 Voltage/Time relation

The first experiment concerns the voltage-time relation. As different scans need different measurement durations the passage time depends on the task. A blank scan with a scan period of roughly 20 min requires a lower voltage than a transmission scan of approximately 4 min. Another idea is to use the same voltage for every scan and vary only the number how often the pellet travels through the liquid drive.

As in the beginning of this thesis the lightbarrier system has not been available, the pellet was clocked by hand. The lowest possible voltage to start the pump is 0.55 V, to move the standard pellet at least 1.8 V are necessary. Increasing voltage leads to faster movement of the pellet. The maximum voltage is 18 V above this value the go-through time does not decrease. Turbulent movement in the hose at laboratory conditions starts at approximately 8 V. Measurements started at a voltage at 2 V and were taken in both directions. The highest voltage tested was around 16 V. Relevant for the PET/MRI head coil system are especially scan times close to 20 min which are used for the blank scan as well as duration around 4 min

4 Results and Discussion

for the transmission scan. The third interesting range deals with go-through times of less than one minute which can be used in both scans by changing direction and repeating them 20 times in the blank scan and 4 times in the transmission scan.

Figure 4.1 shows that the time does not linearly decrease with increasing voltage. Low voltages U implement a maximum scan time t of 1000 s and vary heavily even for exactly the same voltage. The given durations are only regarding the helical path around the PET/MRI head coil. As slight voltages changes already have an influence on the scan time at low voltages, inhomogeneities of the voltage source lead to deviations of up to 50 s between scans with similar voltage at start. Additionally, the output of the voltage source decreases slightly with time which means if a voltage of 2.06 V has been applied at the start, it can fall down to below 2 V until the pellet reaches the final position.

For voltages between 2 V and 3 V small differences in the voltage lead to severe changes. The scan time for 2.5 V already reduces the time to 600 s, for 3 V a scan time of below 400 s is achieved. Furthermore the front end of the pellet has more influence on the movement as for higher voltages (details see Sect. 4.4). This range has been used for blank scans because only those scans last around 20 min.

Transmission scans with a scan duration of around 4 min need higher voltages. The range used for this scan type lays between 4 V and 6 V. While 4 V still have a scan duration of approximately 240 s, 6 V reduce it to the half of it. As visible in Figure 4.1 the reduction with increasing voltage is much lower than before. Furthermore slight changes in the voltage output have less effects on the velocity. Although scan time is already reduced to a tenth of the maximum scan time, the flow in the system is still laminar.

The last important range starts at 8 V because above that border the flow is turbulent. Turbulent flow is more consistent than laminar flow. The duration of a scan falls to less than 80s with a minimum scan time of 36 s for voltages above 15 V. Measurements has been taken up to 16 V but beside quick changes in the voltage output also air bubbles in the liquid drive appeared. Those bubbles can lead to wrong detections of the lightbarrier system as well as they influence the consistency of the pump by reaching it during the scan. For that reason the highest possible voltage applied should stay below 12 V which is also the maximum input in the “Initial Parameters” window of the lighthbarrier software.

Measurements has been mainly taken with voltages U around 2 V, 4 V and 10 V. In Table 4.1 the average scan time as well as its main purpose are visible. With higher voltage the velocity increases which implements a decrease of the scan duration. Furthermore the standard deviation σ falls with increasing voltage output. On the other hand fast movement implements direction changes during

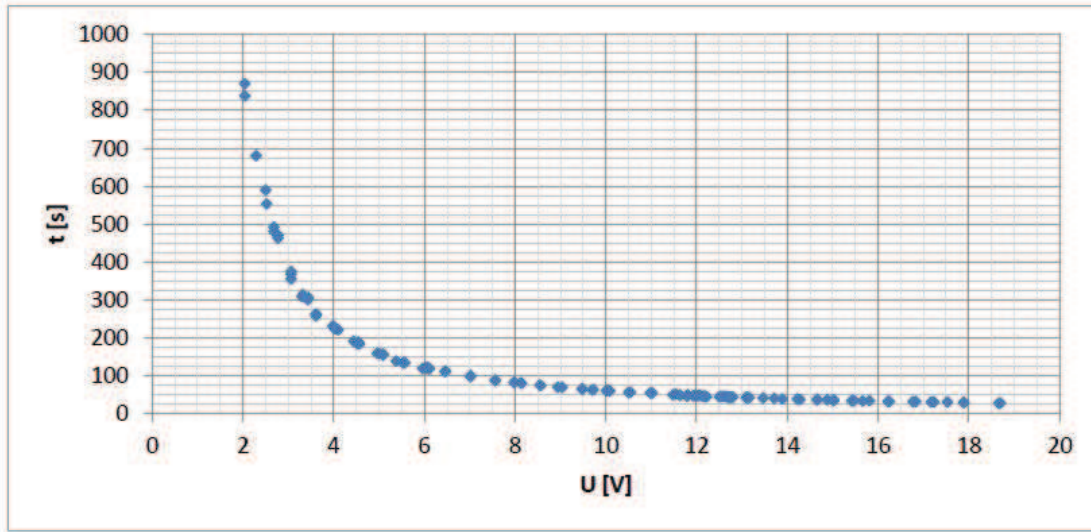


Figure 4.1: Time-Voltage relation for the part around the PET/MRI head coil in the liquid drive.

Purpose	U[V]	t[s]	σ [%]
Blank Scan	2.04	1039,56	4,48
Transmission Scan	4.03	240,61	1,34
Turbulent Movement	10	62,24	1,05

Table 4.1: Summary of the main parameters used for further measurements. Results of measurements from Section 4.5 are also taken into account for these results

a scan where the voltage source has to be turned off for a short period to turn the three-way valves before turning on the voltage source again. Besides loss of scan time this leads to voltage inhomogeneities because it is quite difficult to reach exactly the same voltage again within the short time from the connecting pieces to the PET/MRI head coil. Furthermore all scans must be synchronized afterwards to receive a proper result.

All these measurements has been done in the laboratory at a room temperature of 23°C or more. The room temperature in the PET/MRI room lies between 19°C and 20°C which means a change of up to 10% in the kinematic viscosity. As it is higher for lower temperatures as visible in Table 2.2 the Reynolds number for the same velocity is smaller. Therefore a higher velocity is required to reach turbulent flow. Furthermore, this leads to differences in the velocity for the same voltage in those rooms. To reach the same go-trough time at lower temperatures a higher voltage is needed.

Some examples of tests in the PET/MRI room are visible in Figure 4.2. As the PET/MRI room is usually not available, the number of data points is this figure

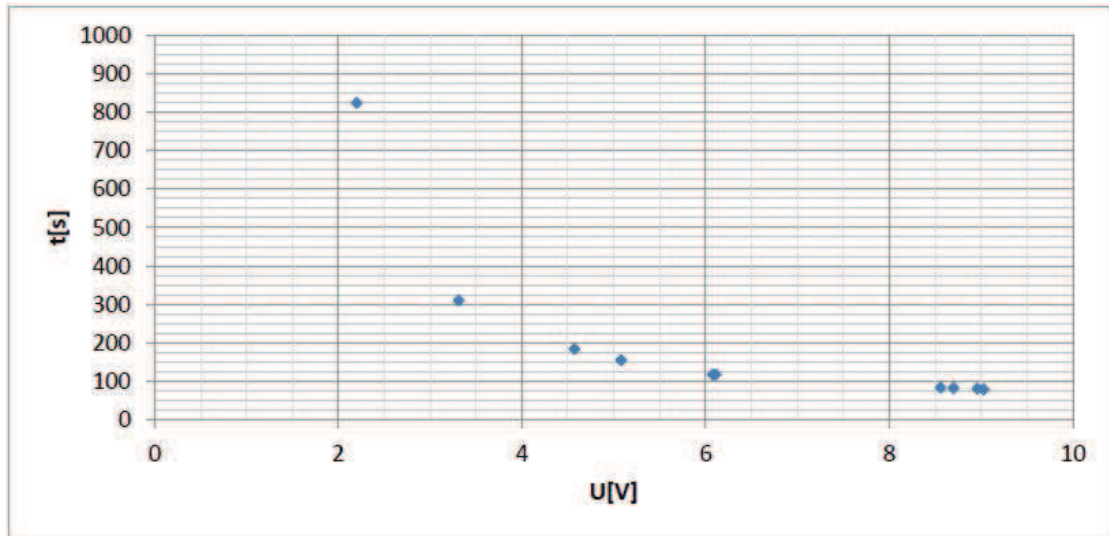


Figure 4.2: The relationship between time and voltage at the conditions in the PET/MRI room. Especially in the area of turbulent flow the scan duration is higher than in the warmer laboratory.

is quite low. Comparing the results with the values in Figure 4.1 differences of up to 10% are visible in the area where turbulent flow appears while for laminar flow the scan times do not vary that much. Preparing a scan at the PET/MRI must take this circumstance into account especially when acting at high voltages.

4.2 Loss of pressure in the liquid drive

This section deals with the loss of pressure in the liquid drive for different velocities in the different components. Additionally, it shows in which components laminar and where turbulent flow is present. Furthermore, the temperature dependence of the dynamic viscosity is discussed shortly.

As already mentioned in Section 2.5, the kinematic viscosity has a big influence on the sort of flow present in the system. Table 2.2 shows that higher a temperature leads to a decrease of the kinematic viscosity. Inserting this in Equation 2.9 this means that the critical value for the Reynolds number is achieved with lower velocities for higher temperatures. In the following calculations a temperature T of $T=23^{\circ}\text{C}$ is assumed in the laboratory. Although it is quite constant in this room, experiments at the PET/MRI have to consider the circumstances there. In fact this affects the velocity and therefore the scan time.

To calculate the total loss of pressure the sum of the losses of every component is taken. The used components are listed in Table 3.1. The value for the tube considers a length of 32 m and in all components a ϵ of 0.0014 mm is assumed. As

4.2 Loss of pressure in the liquid drive

Component	n	δp [Pa]	v [m s ⁻¹]	Re	Flow
Tube	1	19413.8	0.497	4256	t
Necking piece entrance	8	85.2	0.497	4256	t
Necking piece exit	8	74.6	0.884	5678	t
Compensating reservoir entrance	1	16.0	0.497	4256	t
Compenstaing reservoir exit	1	22.2	0.318	3404	t
Curvatures in direction control	2	81.9	0.884	5678	t
Total loss of all components	-	20894.5	-	-	-

Table 4.2: Loss of pressure δp for the maximum flow volume of the pump. In this case the flow in all segments is turbulent (t).

Component	n	δp [Pa]	v [m s ⁻¹]	Re	Flow
Tube	1	9328.7	0.323	2766	t
Necking piece entrance	8	36.01	0.323	2766	t
Necking piece exit	8	31.53	0.575	3693	t
Compensating reservoir entrance	1	6.75	0.323	2766	t
Compenstaing reservoir exit	1	9.38	0.207	2216	m
Curvatures in direction control	2	34.60	0.575	3693	t
Total loss of all components	-	9954.3	-	-	-

Table 4.3: Loss of pressure δp in the fast scanning mode at 10 V. Turbulent flow (t) exists in this case as well as a mixture of turbulent and laminar flow (m).

the pump is seen as a black-box, the expansion and necking between 6 mm and 90 mm are not regarded in the calculations. The Tables 4.2-4.5 present the loss for different voltages of the power source. The first column shows the component followed by the number of appearances and the loss for one of these components. Furthermore the velocity and the Reynolds number are given in this table. The last column determines if laminar (l) or turbulent (t) flow is existent. For Reynolds numbers between 1800 and 2300 a mixed (m) state is present.

The base for the flow velocity is the speed of the average pellet within the liquid drive. Due to friction the actual flow velocity of the water is slightly higher and so is

Component	n	δp [Pa]	v [m s ⁻¹]	Re	Flow
Tube	1	1243.4	0,083	714	l
Necking piece entrance	8	2.40	0.083	714	l
Necking piece exit	8	2.10	0.148	950	l
Compensating reservoir entrance	1	0.45	0.83	714	l
Compenstaing reservoir exit	1	0.63	0.053	571	l
Curvatures in direction control	2	2.31	0.148	950	l
Total loss of all components	-	1285.1	-	-	-

Table 4.4: Loss of pressure δp in the transmission scan mode at 4 V. The flow is laminar l for all components in this case.

4 Results and Discussion

Component	n	δp [Pa]	v [m s ⁻¹]	Re	Flow
Tube	1	288.2	0.019	165	l
Necking piece entrances	8	0.129	0.019	165	l
Necking piece exits	8	0.113	0.034	220	l
Compensating reservoir entrance	1	0.024	0.019	165	l
Compenstaing reservoir exit	1	0.034	0.012	132	l
Curvatures in direction control	2	0.124	0.034	220	l
Total loss of all components	-	290.4	-	-	-

Table 4.5: Loss of pressure δp in the blank scan mode at 2 V. The flow is laminar l for all components in this case.

the total pressure loss. Calculations follow Equation 2.10 for the tube and Equation 2.14 for the different components. As the pressure loss is directly proportional to the square of the velocity it decreases with decreasing voltage.

The main part of the loss appears in the tube itself due to the length of this component. The percentage for this component of the total loss increases with decreasing voltage. At a voltage of 2 V (Tab. 4.5) more than 99% of the total pressure loss happen in the hose while this component is only responsible for approximately 93% at full speed (Tab. 4.2).

From the other components the necking pieces plays the most important role in the tables above followed by the 90°-arches in the direction control. In the necking pieces the sudden narrowing causes a higher pressure loss than the enlargement of this component. Each of these components disturbs the flow about the doubled amount as the arches and in contrast to them they are present 8 times while there exist only 2 curves in the liquid drive. Because of its bigger diameter the compensating reservoir has the least impact on the loss of pressure. Here the narrowing appears at the exit of the component which implies a higher loss there than at the entrance.

Beside the velocity the Darcy friction coefficient influences the loss of pressure. As visible in equation 2.11 it is indirectly proportional to the Reynolds number for laminar flow while there is another limiting factor for turbulent flow. The higher the velocity the smaller gets the Darcy friction coefficient.

At full speed and with 10 V flow is turbulent (Tab. 4.2-4.3). The only exception is the compensating reservoir at 10 V which is already in the mixed zone. Due to the continuity equation and the higher diameter in the compensating reservoir the Reynolds number falls slightly below 2300. The situation at 4 V and 2 V (Tab. 4.4 and 4.5) is completely different. For these velocities laminar flow predominates and the Reynolds number is below 1000 for every component.

l[m]	[°]
0,0028	1
0,0140	5
0,0279	10
0,1257	45
0,2513	90
0,5027	180
1,0053	360

Table 4.6: Comparison between distances l in [m] and round segments in [°]

In Tables 4.2-4.5 the velocity is given in ms^{-1} but for localizing the pellet in the liquid drive this is not helpful. The distance covered in degrees is of far more relevance for further calculations. Table 4.6 compares the measured distances in meters to the path covered in degrees in the helical part of the hose around the PET/MRI head coil. Checking the velocities in Tables 4.2-4.5 shows that at full speed nearly half a round is covered in 1 s. In the fast scanning mode the average speed is approximately $115 [\text{s}^{-1}]$ which implies round times of slightly more than 1 s and a total go-trough time of one minute. In the transmission scan mode the pellet runs through approximately 30° in 1 s while in the blank scan mode only a distance of less than 7° is covered.

Velocities in the other components are not further regarded because the pellet does not pass by and the distances covered within the inner diameter of 6 mm and 10 mm are negligible compared to the length of the hose.

The first entry in Table 4.6 is approximately the minimum resolution of the PET. This value is mainly relevant for the step-size in the output data of the lightbarrier software.

4.3 Filling of the pellet

This and the following sections deal with the movement of the pellet inside the helical part of the hose. In a first step the amount of fluid was determined and the ideal result is presented in table 3.4. As it is quite difficult to fill in the ideal volume, measurements with divergent amounts have been made. This section discusses the dependence of the movement regarding different filling volumes and explains which range guarantees nearly equal movement.

According to results of section 3.2 the ideal amount for the used PMMA pellet is $293 \mu\text{l}$ in the testing phase. Therefore, the undertaken measurements deal with volumes between $200 \mu\text{l}$ and $400 \mu\text{l}$ with a step-size of $50 \mu\text{l}$. Furthermore different

4 Results and Discussion

velocities are tested. Voltages used for these measurements are in the range of 3 V to 6 V in steps of 0.5 V.

Figure 4.3 shows the development of the different sectors within one round for different filling volumes in both directions. Therefore sector 1 is always the 1st quarter from the bottom bar to one side and the 2nd one is still ascending up to the top bar. The 3rd and 4th sector are the descending part within the round with the last one ending at the bottom bar again. The deviation is always compared to the mean quarter time within one round and is in a range below $\pm 5\%$ with exceptions in Figures 4.3e and 4.3j. If the value for the deviation is below 0 this implies that the time needed is shorter than the average and therefore the velocity is higher for this sector.

Figures 4.3a and 4.3f show the expected behavior. The deviation is higher for lower voltages because gravity has a bigger impact on acceleration and deceleration within one round there. As only 200 μl of the solution and more than the same amount of air are inside the pellet, it has in total a lower density than the surrounding water and will ascend in sector 1 and 2 if no voltage is applied due to gravity. In sector 3 and 4 this means it moves backwards until it reaches the top position within one round. If a voltage is applied to the system the movement is influenced by this force. As visible in 4.3a and 4.3f the velocity is higher in sector 1 and 2 for both directions. With higher voltage the total velocity of the pellet is higher which leads to less influence of the gravity. While in both directions the same sectors are above and below the mean, the ranking which sector is the fastest and which is slowest changes with the direction in this case. This effect will be discussed in detail in Section 4.4.

The fast movement for the 3rd segment at higher voltages in 4.3a results from the high velocity in the section before. The maximum speed for a pellet with a filling volume below the ideal one is reached at the top position in the circle. At small voltages deceleration quickly happens which leads to the expected result while at higher voltages this effect persists in the descending sector as well. This effect will appear again at filling volumes above 350 μl .

With 250 μl of the solution and only 160 μl of air the pellet is closer to floating. In Figure 4.3b again at low voltages the ascending sectors are faster than the descending but the deviation decreased already to approximately 2% at 3 V compared to nearly 5% at 200 μl . Beginning with 3.5 V the deviation is below $\pm 1\%$ for each sector. While sector 2 is the fastest sector until 4.5 V its velocity is even below the descending sectors for higher voltages and sector 1 takes its position as fastest sector. Due to the deceleration the 4th sector is the slowest for lower voltages,

while it has a slightly higher velocity than the 3rd sector at higher voltages when the thin end is the leading end in the movement.

The results of the measurements for 250 μl with the thick end frontwards are plotted in Figure 4.3g. At lower voltages the deviation is higher than in the other direction. Again the velocity is higher in the ascending sectors and for higher voltages the deviation falls below $\pm 1\%$ of the average speed for all sectors. In contrast to 4.3f the 2nd sector is the fastest and the 4th is the slowest up to 4.5 V.

At a filling volume of 300 μl of solution the pellet stays in suspension in water. For this volume the most consistent movement is expected. Figure 4.3c shows the desired behavior for the whole range of voltages. The average of the ascending part and the descending part is close to the 0-line and the deviation for nearly all dots is within the range of $\pm 1\%$.

With the same filling volume the other directions shows a completely different behavior (Fig. 4.3h). In this case the 1st sector is the fastest for all voltages while the 3rd one is the slowest. Additionally, the deviation is much higher in this direction than with the thin end frontwards. It is interesting that the upper half, which is sector 2 and 3, is much slower than the lower one, which is similar to movement at high voltages with a raised filling volume. Additionally, the deviation is not decreasing with increasing voltages. The behavior in total looks more alike the one of pellets with a raised volume than pellets with a lower amount inside.

If there is more liquid inside the pellet than ideally proposed, the pellet sinks towards the bottom bar if no voltage is applied. The uplift force of the air inside is not able to compensate the gravity force of the fluid combined with the pellet material. This leads to the expectation that the pellet travels faster in the descending sectors in this state. In 4.3d it is already visible that for small voltages, the green and violet dots stay below the 0-line which implies that the speed of the pellet is higher in these sectors than in the ascending sectors. Again the deviation becomes smaller with increasing voltage and is below $\pm 2\%$ for all measured velocities.

While moving with a filling volume of 350 μl of solution and the thick end frontwards (Fig. 4.3i) the 2nd sector is the slowest and the 4th the fastest for low voltages which is similar to the other direction. The other parts in the round have changed their position in the ranking. At voltages above 4 V the situation changes and the starting sector has the highest velocity while movement in the 3rd one happens with the least average speed. The deviation is calculated with approximately $\pm 3\%$ for low voltages at the extreme sectors and falls to $\pm 2\%$ for higher voltages.

4 Results and Discussion

As already mentioned above, the slow movement of the 2nd sector persists in the beginning of the next one and leads to a slower average velocity in this segment than in the one which starts with the maximum velocity at the bottom bar. Although acceleration starts in this sector it does not reach the average of the 1st one for high voltages. In the other direction with the thick end frontwards this effect even leads to the highest average velocity in the segment which starts at the lowest point of the circle.

For the full pellet the ascending part with the thin end of the pellet frontwards is much slower than the descending half in the liquid drive. Beside the deviation, which is above $\pm 5\%$ for 3 V movement, the behavior in Figure 4.3e can be compared to the one in Figure 4.3a except with changed sign. In this case the last sector is by far the fastest followed by the other descending part. The sector from the side to the top needs longest. By increasing the voltage the deviation falls again to $\pm 2\%$ and below for all sectors.

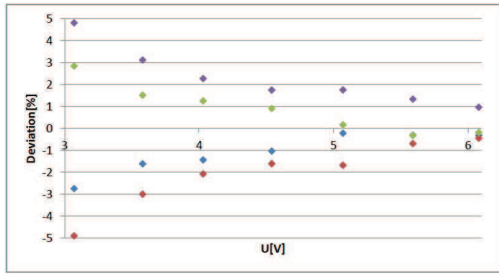
The last subfigure (Fig. 4.3j) shows the behavior for the movement of a full pellet with the thick end in front. Here again the 2nd sector is the slowest one especially for low voltages. Starting with a voltage of 3.5 V the average velocity in sector 1 becomes higher than the one in sector 3. This persists also for high voltages, where the velocity in the 1st segment even reaches the one of the last sector. The deviation falls as in the other direction from more than $\pm 5\%$ of the average velocity for two sectors to below $\pm 2\%$ for all sectors with increasing voltage.

The behavior explained for the 350 μl filling is also valid for the full pellet. While at low voltages the deceleration happens within the sector starting at the bottom the average velocity for the 3rd segment becomes the lowest for high voltages because the speed maintains throughout the decelerating part.

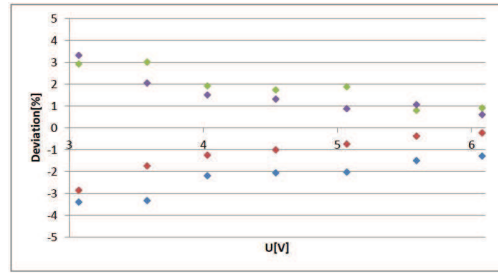
Additionally to the measurements shown in Figure 4.3, an experiment with a voltage of slightly above 2 V has been undertaken. The deviation therefore towards the travel reached up to $\pm 18\%$ for the last ascending respectively descending segment at a filling volume of 200 μl which means the highest average velocity is approximately 1.5 times the lowest one. At filling volumes above 350 μl again the same numbers are possible. By reducing the gap to the ideal filling this ratio is decreasing dramatically. The best result available at 300 μl still has a value 1.09 but also at 250 μl and 350 μl the ratio stays below 1.2. As ideal filling is quite difficult to achieve and the acting with the radioactive source should take as less time as possible, the volume of the solution inside the pellet should move within that range.

These measurements mainly represent the testing phase of this project because in the final version the liquid drive will contain heavy water instead of distilled

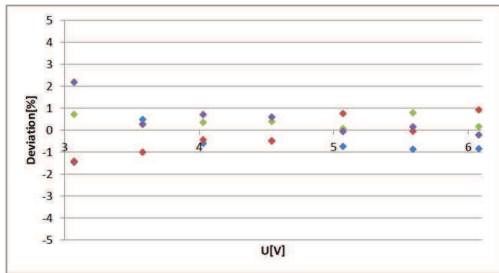
4.3 Filling of the pellet



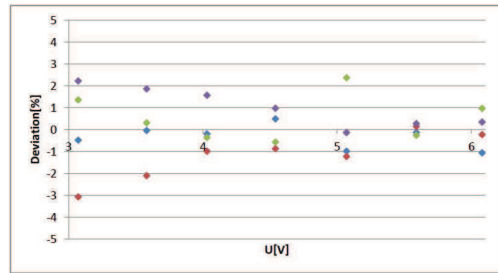
(a) 200 μ l thin



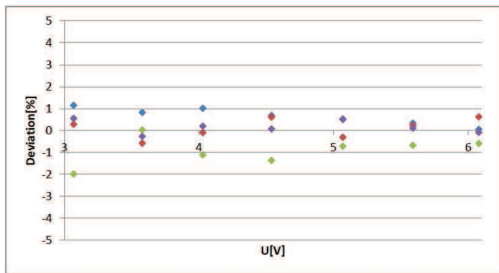
(f) 200 μ l thick



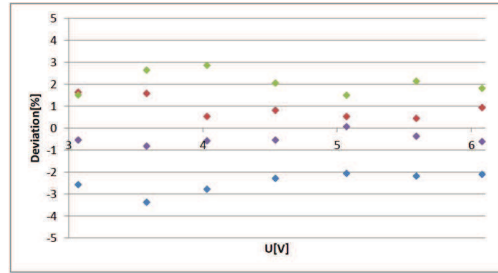
(b) 250 μ l thin



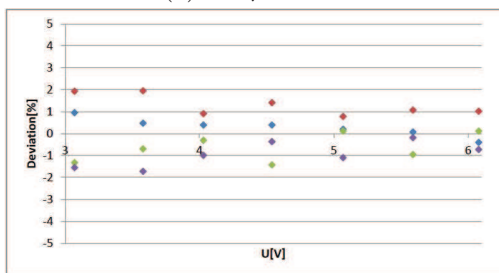
(g) 250 μ l thick



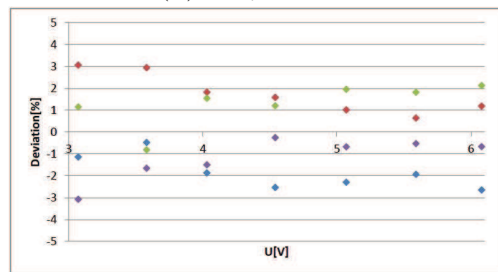
(c) 300 μ l thin



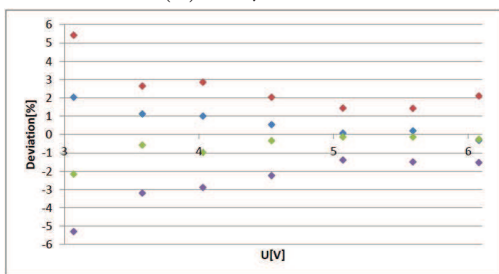
(h) 300 μ l thick



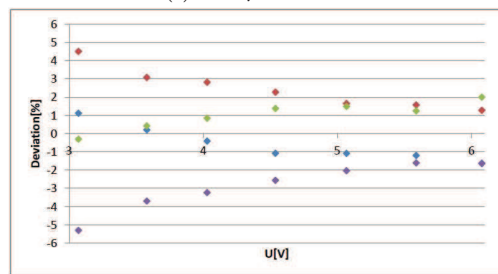
(d) 350 μ l thin



(i) 350 μ l thick



(e) 400 μ l thin



(j) 400 μ l thick

Figure 4.3: Deviation of different sectors for different filling volumes at different voltages. Sector 1 is always marked in blue, sector 2 in red, sector 3 in green and sector 4 is the violet dot in each plot. “thin” means the sharp end of the pellet is in front of the motion, while “thick” implies the same for the flat.

4 Results and Discussion

water and the ideal filling volume will be a nearly full PMMA pellet. This means if this pellet is kept also for the final version, filling volumes above the ideal state are hardly possible. Nevertheless these experiments show that the traveling of the pellet strongly depends on its density and can lead to an inconsistent movement within the liquid drive if the filling is messed up.

Details to the movement within one round for a nearly ideally filled pellet are given in the next section. Absolute values of the dots in Figure 4.3, which represent the mean of all measurements are visible in the appendix in Section A.2.

4.4 Movement within one round

This section deals with the movement of the pellet inside the circles of the liquid drive. As mentioned in the section before, even for a perfectly floating pellet consistency in quarter velocities is not given. Therefore a detailed analysis of the travel within the liquid drive has been made. In one measurement 3 consecutive rounds have been equipped with fiber cables and additionally at both ends of the liquid drive fiber cables have been attached to the PET/MRI head coil system to compare the velocity of the measured segment to the average velocity in the whole system. For better comparison each segment has been tested 5 times in both directions for 3 different voltages. The voltages used in this experiment have been the same as in Section 4.2.

The numbering of the sectors is the same as in the previous section. This means sector 1 and 2 are the ascending sectors in both directions while sector 3 and 4 are descending. In contrast to the previous section in the following diagrams the correction factor is given. The program uses this factor to calculate the actual velocity for every sector. Therefore it uses the average speed within two neighboring fiber cable positions and adjusts that value by the correction factor which depends on the position within the round. If every position is identified this factor is calculated twice in each measurement for every sector. Consistent movement implies that this factor is 1 for every quarter but as already registered in the previous section, this does not work out.

Figures 4.4-4.6 show the collected results in form of a boxplot. In this type of figure the lower line of the box represents the value of the 1st and the upper line the value of the 3rd quartile. The median is also shown in these plots. The values outside the box show the minimum and maximum measured within this experiment. Due to the number of repetitions in total 100 values are taken into concern. At 2 V the measured correction factor varies between 0.85 and slightly above 1.1 which

4.4 Movement within one round

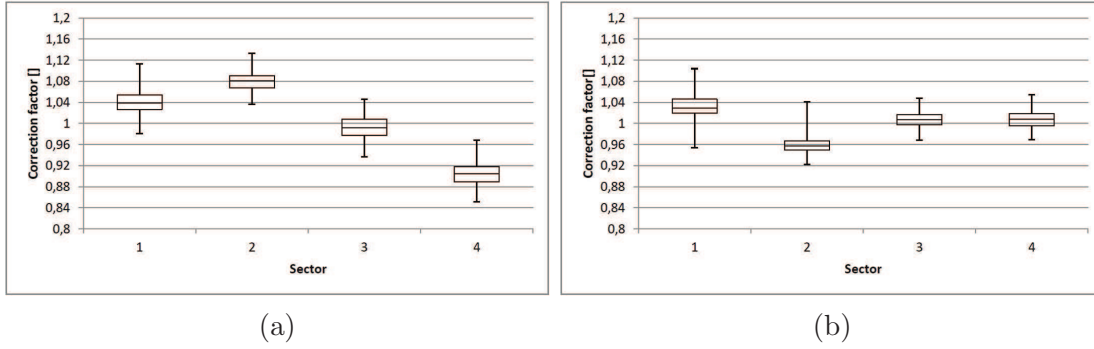


Figure 4.4: Quarter coefficients for the different sectors at a voltage of 2 V. (a) represents the values with the thin end frontwards, (b) shows the results for the thick end frontwards.

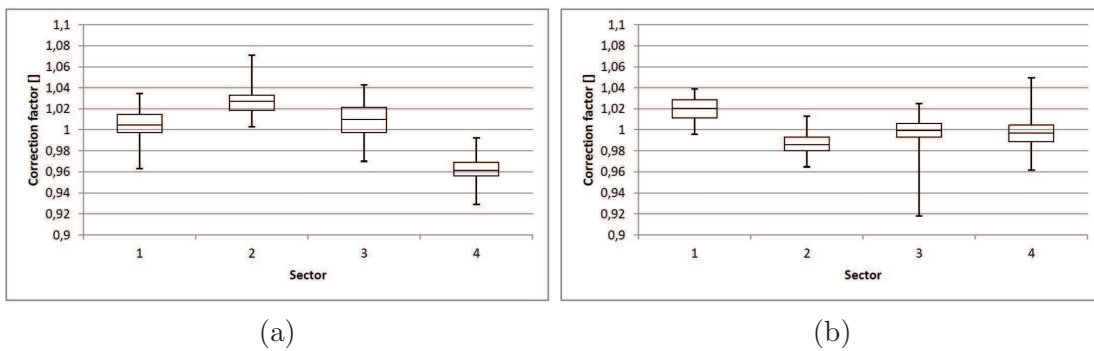


Figure 4.5: Quarter coefficients for the different sectors at a voltage of 4 V. (a) represents the values with the thin end frontwards, (b) shows the results for the thick end frontwards.

leads to a different range at the y-axis in this plot compared to 4 V and 10 V. A coefficient above 1 means a higher velocity in this sector than average within the round because the mean velocity of the segment is multiplied with this factor.

For all measurements the same filling volume has been used, which has been approximately the floating volume of $293 \mu\text{l}$. A comparison of Figure 4.4a-4.6a shows that all 3 plots have the same shape. The 1st sector has a velocity which is close to the average speed of the whole circle or slightly above. In the 2nd sector the pellet is accelerated independent of the voltage applied only the factor has a broad variation. While at 2 V the average velocity in this sector must be multiplied with approximately 1.08 this factor decreases with increasing voltage to below 1.02 for the fast measurements. Regarding the doubled range for 4.4a the boxes in both sectors are nearly doubled as broad as at the other voltages.

In the 3rd sector the pellet is slower than in the previous sector. While at 2 V and 10 V the correction factor is slightly below 1 meaning a lower speed than in average, at 4 V the velocity is still higher. In the last sector the velocity falls below the average one for every voltage and has the biggest deviation compared to the

4 Results and Discussion

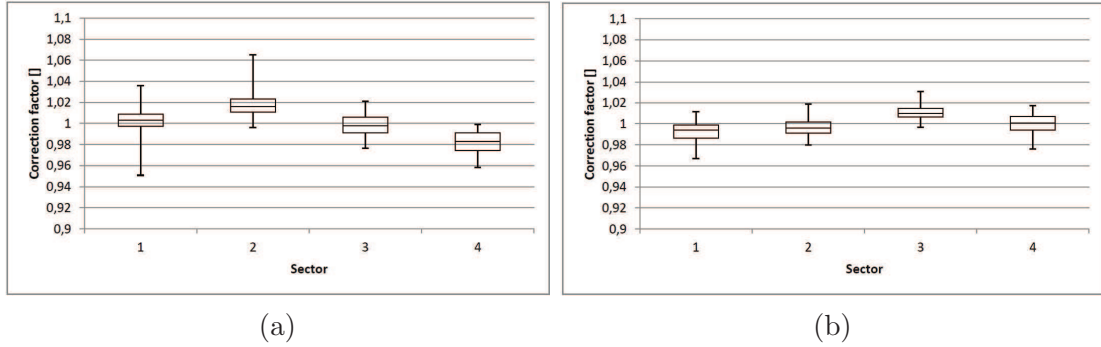


Figure 4.6: Quarter coefficients for the different sectors at a voltage of 10 V. (a) represents the values with the thin end frontwards, (b) shows the results for the thick end frontwards.

mean velocity. For 2 V the median of the correction factor is at 0.91 which means a huge reduction of the speed in this section. At higher voltages the correction factor increases, resulting in a value of slightly above 0.98 for 10 V.

In the other direction, presented in Figures 4.4b-4.6b, the movement at 2 V and 4 V is more or less the same whereas at 10 V differences appear. At 2 V as well as at 4 V the 1st ascending sector is the fastest with a correction factor of slightly below 1.04 respectively 1.02. In the following sector the velocity decreases to the minimum in each round leading to a correction factor of below 1. In the other sectors the pellet travels with approximately the mean speed.

At 10 V and the thick end frontwards the situation changes. Here, the lowest velocity is given in sector 1 and increases to the average in sector 2. In the 3rd sector the pellet accelerates once more while it travels with the mean speed again in the last sector. All the values for the correction factor normally vary between 0.99 and 1.01 which means that nearly consistent movement is given for this voltage with the thick end frontwards.

Overall motion with the thick end frontwards is more consistent than in the other way at every voltage. It is not only that the median of the correction factor is closer to 1 for all measurements, additionally also the boxes are more compact than with the thin end frontwards.

While the dispersion in Figure 4.4 can be explained by fluctuation of the voltage and even a very detailed evaluation shows no further structure in the motion of the pellet, the large deviation especially in 4.5b and 4.6a appears not randomly. In both cases these values derive from the same position which is the 10th round frontwards and respectively the 11th round backwards. At this position the furthest distance to the pump is given which means that between up to this point the water is ejected while afterwards it is sucked by the pump.

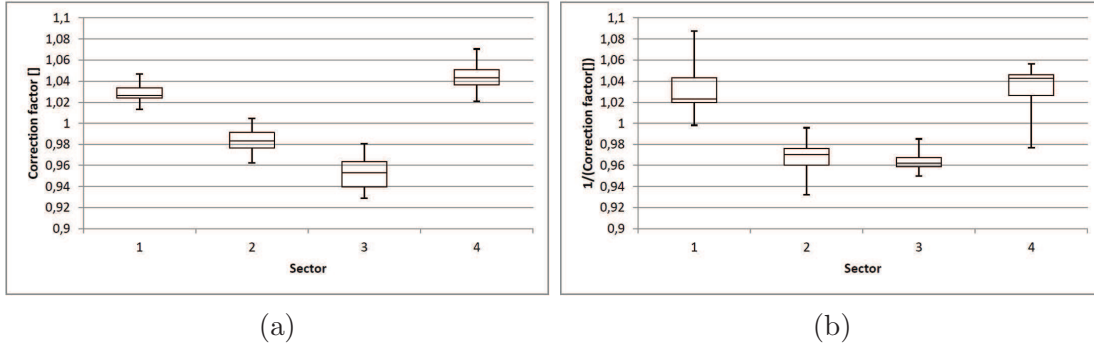


Figure 4.7: Effect of the torsional momentum on the pellet motion. Indirect proportionality of the quarter coefficients is given because it leads to promotion in one direction while it constrains the movement in the other way. (a) shows the correction coefficients with the thick end frontwards, while (b) presents the reciprocal correction coefficient of the thin end frontwards.

As a next step the inconsistency of the movement has been observed. Even for an ideally filled pellet differences in sector velocities appear. If only gravity influences the movement, the curve must be the same in both directions but as visible in the figures 4.4-4.6 the motion varies for the different directions. This implements that there is an additional force which depends on the front end of the pellet - the torsional momentum. If the floating pellet is put in horizontal position in a cup of water it always turns into an upright position with the screw on the top because the thin end has a lower density than the thick end. In the beginning, there is only a slight difference due to the screw but when the air bubble in the pellet also moves upwards this effect is supported. The force effects the pellet depending on its position but while it promotes the motion in one direction it constrains the movement in the other way.

Regarding Figure 4.4 and 4.6 this indirect proportionality can be already assumed. A more obvious evidence has been achieved by putting the whole mass to one end of the pellet. Therefore a copper wire has been fixed at the end of the screw while the pellet itself has been empty. In water it floats but turns immediately. Measurements have been done again for 3 different voltages with the same result. Figure 4.7 shows the boxplot for the 4 V measurements where the correction coefficients of the thick end in front (Fig. 4.7a) is compared to the reciprocal correction coefficient of the thin end frontwards (Fig. 4.7b). The structure appears quite similar and is also present at higher and lower voltages. Of course accelerating the pellet reduces the deviation of the correction factor again.

Summing up this section it is clear that the dispersion of the correction factors approaches to 1 by increasing the voltage. Especially at low voltages big differences in this coefficients can appear due to inhomogeneities in the voltage output,

which affect the velocity far more in these measurements than at higher voltages. Regarding these facts the correction coefficients are important for determination of the pellet position in the liquid drive. Although every section is only measured twice in a regular scan, improvement compared to no correction factor is given.

4.5 Consistency of round time

This section deals with the consistency of the round times and if it is necessary to introduce an additional correction factor which depends on the round number in the liquid drive. Therefore 10 measurements in each direction for the 3 selected velocities have been made with all 16 fiber cables at the bottom bar. The cables have been arranged at each pair of holes except position 5,6,10,14 and 15 which means 15 round velocities are given in each measurement. Afterwards the different rounds are normalized to the average velocity of the whole scan. Figure 4.8-4.10 show the results for these experiments where (a) always represents the factors for the thin and (b) for the thick end frontwards. All values represent the mean with its standard deviation. As already in the sections before, the range on the y-axis is doubled for the 2 V measurements in comparison to the others.

The results for the measurements with 2 V are presented in Figure 4.8. In both directions and for all positions in the liquid drive, the mean correction coefficient is between 0.98 and 1.02. Including the standard deviation at all positions the mean value is within the possible range. The reason for the high standard deviation in the experiments with 2 V is again based on the inhomogeneities in the voltage output which have more influence at low velocities. Especially plot 4.8a shows the decreasing of voltage over time mentioned in Section 3.1.1 which leads to velocities below the average one in the last rounds. In the other direction the fastest rounds are also in the beginning. Overall no distinct structure is given which means that the spreading of the velocities is randomly. Furthermore, it is visible that there is no difference concerning the direction.

The same is valid for the rounds in the transmission scan mode at 4 V. The mean values of all measurements vary in the range of 1 ± 0.01 times the average velocity. This can again be explained by the inhomogeneities of the voltage source and is not influenced by the liquid drive itself. This also means that the length of each round in the liquid drive is equal without any traps or inhomogeneities which affect the pellet. Once again the part with the highest velocity is in the beginning and the trend is more or less the same in both directions.

4.5 Consistency of round time

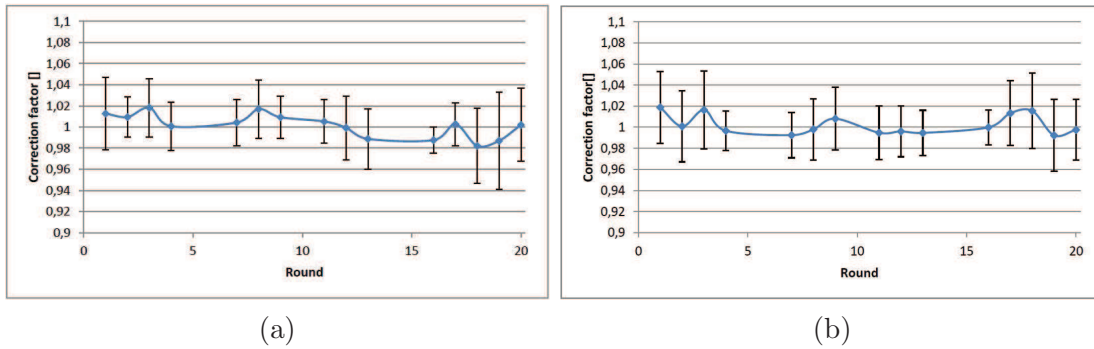


Figure 4.8: Average normalized round times with its standard deviation for a voltage of 2V. (a) represents the thin end of the pellet frontwards, (b) the results with the thick end.

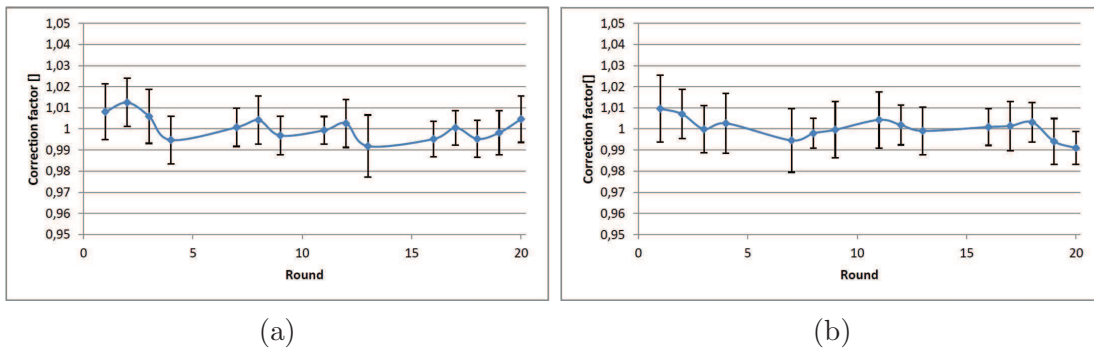


Figure 4.9: Average normalized round times with its standard deviation for a voltage of 4V. (a) represents the thin end of the pellet frontwards, (b) the results with the thick end.

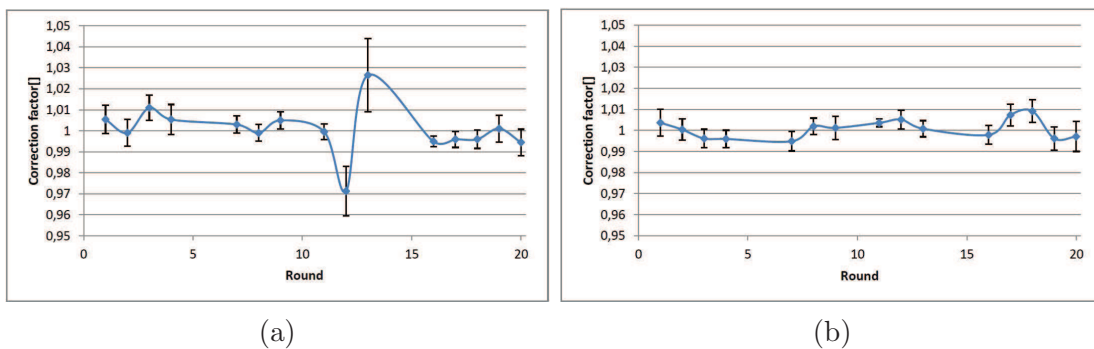


Figure 4.10: Average normalized round times with its standard deviation for a voltage of 10V. (a) represents the thin end of the pellet frontwards, (b) the results with the thick end.

4 Results and Discussion

At the high speed measurement the motion is as smooth as for lower voltages except between the 12th and the 13th round with the thin end frontwards (Figure 4.10a), where the correction factor jumps for more than 3%. First it falls to 0.97 while raising afterwards to 1.03 to equalize the occurred failure again. Not only the correction factor is different from the others in these rounds also the standard deviation is much higher. All other rounds for this as well as all rounds in the other direction have a correction factor close to 1. Additionally, the standard deviation is very low which means that the movement is nearly consistent in all rounds.

In contrast to the correction coefficients for the different quarters, the multiplying factors in round motion are much closer to 1. Additionally, the trend is not the same for different voltages as in the previous section. Therefore no clear prediction for the movement in a defined round is possible. To commit changes of the velocity within a scan average velocities in sectors of a length of 2-3 rounds are used. As the voltage does only slightly change within some time, the velocity does not change dramatically within some time and these effects are absorbed by the average velocities in these sectors. Furthermore, even a filling volume which is out of the proper range does only effect quarter coefficients but has nearly no influence on the consistency of round times.

Although the consistency is given within one measurement, 2 consecutive measurements with the same voltage can lead to different scan times. On the one hand side the value presented on the power supply varies slightly on the other hand there is an influence of the shape of the pellet. At low voltages the duration can vary up to 4s per round which is approximately $\pm 8\%$ of the total round time. At high voltages this effect is suppressed and differences are only in the range of $\pm 3\%$. Nevertheless fast movement leads to direction changes, where the power supply has to be shut off completely and started again after the change has been executed. Within the short period the pellet takes to the 1st position the voltage has to be set again to avoid unequal round times.

According to the facts above the program only uses the sector times which include usually more than one round and the measured quarter coefficients. Additional factors received from this section are not considered.

4.6 Loss of water

Due to the open surface of the compensating reservoir water evaporates over time. While acting with distilled water, this has no further relevance but in the final version it has to be taken into account due to the price of heavy water. The

amount of lost distilled water is approximately 6 ml per day for a full compensating reservoir.

Reduction of this amount can be achieved by 3 ways:

- closing the compensating reservoir
- reducing the open area of the system
- tracing out the compensating reservoir and replace it with a connection piece in the time where the system is not used

The 1st solution leads already to a reduction of evaporation for more than 50% which still means that more than 3 ml per day are lost. Option 2 is a further improvement. Therefore the water in the compensating reservoir has to be depleted and the water has to be restored after the use of the system. This results in a very small open area in the hose itself leading to evaporation of less than 1 ml per day.

As best solution the last option is suggested. Therefore again the compensating reservoir has to be emptied and afterwards it has to be replaced by a connecting piece which can be easily stuck to the open ends of the hose instead. With this solution a closed circle without any open area would exist which would have the advantage of nearly no evaporation as well as less pollution with dust particles.

4.7 Lightbarrier manual

After plugging in the lightbarrier hardware and connecting it to the computer, it is possible to start the software. The GUI of the lightbarrier appears. Possible options at this time are to click the “Settings” button as well the “Cable Positions” button as visible in Figure 4.11. Below, the 3 columns with their slots are present. In total there are 16 rows and in the beginning next to the position in all slots “nothing detected yet” appears. The 1st column shows the number of the fiber cable starting with 0, in the second column the time of the lightbarrier system in μ s is placed and the last column shows the corresponding computer time in ms since start of the day.

While the “Settings” button includes the parameters such as BaudRate and number of Data bits as well as the selected serial port and has already existed by starting with improving the program, the “Cable Positions” button has been arranged during this thesis.

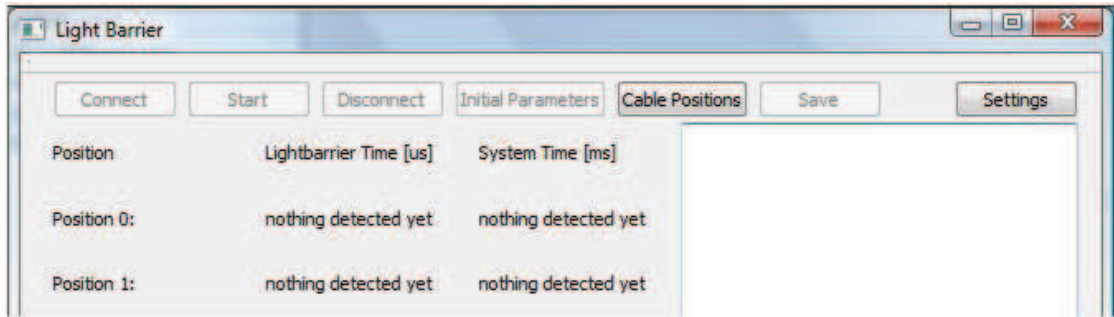


Figure 4.11: Upper part of the GUI after starting the software of the lightbarrier system

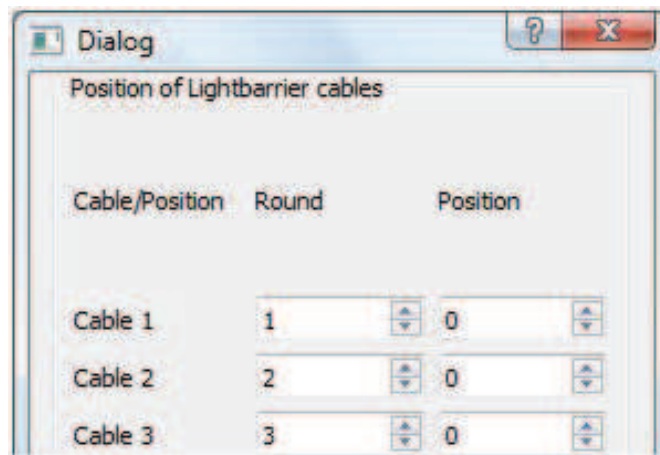


Figure 4.12: Upper part of the “Cable Positions” dialog

In this dialog (Fig. 4.12) it is possible to tell the program at which positions the fiber cables are stuck to the PET/MRI head coil. To the slots in the 2nd column, numbers between 1 and 21 can be assigned. It is the number in which round the cable is moving into. The 1st position in the liquid drive is in round 1, for the last position as start of the 21st round the number in this column has to be set to 21. As the pellet enters the liquid drive in the back when traveling frontwards the numbering also starts in the back.

The last column gives the position within the round and varies between 0 and 3. This number defines the bar the cable is attached to. For the bottom bar (C-bar) the 0 must be assigned and then it goes counter-clockwise in the direction of the B-bar, which gets a 1, to the top bar (A-bar) and finally to the D-bar for the 3.

The preset parameters contain the start and the end of the liquid drive as well as 2 complete rounds with fiber cables arranged at 5 consecutive positions to have the possibility of calculating the quarter coefficients. The remaining 4 cables are assigned to positions between those rounds.

The positions set in this window should be ascending, which means that the 1st

Code segment 4.1: Defining the numbers of the “Position” vector

```
currentPosition.Position1 = 360*(ui->cable1Box1->value()-1)
+90*(ui->cable1Box2->value());
```

cable should have the lowest round number. By clicking the “Apply” button the assigned positions fill a “Position” vector with the numbers of places is calculated to degrees. Therefore 1 is subtracted from the number of the first column and this number is then multiplied with 360. Afterwards the assigned number in the last column is multiplied with 90 and added to the previous number as visible in code segment 4.1. This is done for all 16 positions.

Clicking the “Cable Positions” button also enables the “Initial Parameters” button. By opening this dialog the parameters used for the scan are determined. As visible in Figure 4.13 the user has to deal with the voltage as well as with the direction of the scan and the front end of the pellet. The range for the voltage slicer is between 1.8 V (1800 mV) and 12 V (12000 mV) and the determined value is mainly used as a hint in the output file as well as a first velocity prediction.

In the left box the user can distinguish the flux direction. “frontwards” means the direction from the compensating reservoir to the PET/MRI head coil. In this direction the output file counts from 0 to 7200 degrees and the pellet travels from the backside of the head coil frontwards. Respectively “backwards” means exactly the opposite. In many “if” functions in the program the direction determines which part of the function is used.

The right box in this window respects the front end of the pellet in flow direction. Here the user has the decision between the flat end which is called “thick” in this box and the sharp end with the screw at the top, where the user has to tick the “thin” button. This box determines which timestamp at each position is taken in calculations for the output file. Ideally 2 timestamps are given when the pellet passes by a position with attached fiber cables, one in the pellet reaches the position and another when it is finally passed by. As the detection at the thin end is not as consistent as on the other side the program only uses the timestamps of the flat end in its calculations.

Preset parameters here are a voltage of 1.8 V in frontwards direction with the thin end in flux direction.

Afterwards the “Connect” button is enabled. By clicking this button the system starts to show the time passed by since plugging in the device in seconds in the white window on the right side of figure 4.11 and additionally enables the “Start” as well as the “Disconnect” button. If the pellet is detected at a position, it also

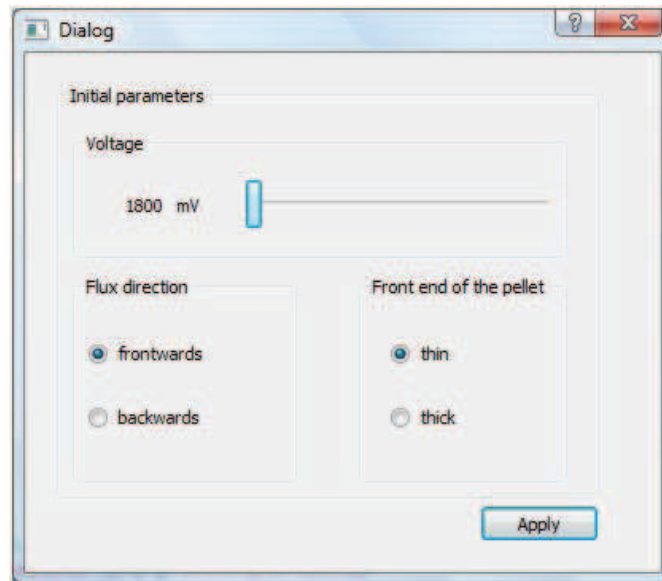


Figure 4.13: The “Initial Parameters” dialog of the lightbarrier system

appears in this window by showing position and the timestamp of the lightbarrier system in μs . The position is presented as 2^n where n is the number of the position. Furthermore the last timestamp of each spot is set into the lines on the left side instead of the “nothing detected yet” phrase which means it is easily visible which position failed in detecting the pellet. By using the “Start” button the detection is set back to the phrase.

As long as only 4 or less timestamps are recognized at the same time the lightbarrier time and the computer time are synchronized. If more detections happen at more or less the same moment further detections are stored in the buffer and are presented with a delay. As the signal for the computer time is the transmitting of the timestamp to the computer, it can be belated too while the lightbarrier time has the right value. By clicking the “Disconnect” button and connecting afterwards again this time delay can be avoided. In further calculations this effect does not matter because it uses only the 1st computer time as a reference and uses the time differences of the lightbarrier system time for further use.

If the pellet is detected and this is shown within the system, it is possible to save the received data by pushing the “Save” button. This order instructs the program to do all the calculations to provide the data for the output file. In this file in the first row the initial parameters given in the corresponding window are present followed by the total time elapsed between the 1st and the last detected position. Then the starting position is given and beside it the timestamp of the lightbarrier system and the time at the computer. The next calculated position is placed below again with its corresponding timestamps until the final position is reached. The

stepsize herefore is about 0.1° .

To review the results also all important parameters as the velocity between neighboring positions as well as the calculated quarter coefficients and the arranged cable positions are presented in the end of the file.

4 *Results and Discussion*

5 Conclusion and Outlook

The aim of this project is to develop a new method for attenuation correction in PET/MRI. First tests show already proper results. The system of the liquid drive allows movement of the point source with velocities where the emitted radiation is high enough to achieve a proper count rate but quite low in comparison to an additional CT. Although the motion is not totally consistent within one round and also varies slightly for different rounds a prediction of the location is possible. In the last tests the fast motion of the pellet has been preferred as it is more consistent. The advantages in nearly same quarter coefficients and similar round times superimpose the disadvantage of direction changes within one scan.

The hardware itself fulfills the requirements requested in Section 3.1. Durability of the system as well as easy handling of the pellet is given in all working stages. Additionally, fast direction changes in the system are possible.

The software developed during this thesis allows easy and accurate localizing of the pellet in the liquid drive. At the moment the system is especially useful for time synchronization and for detecting the start and the end of the movement in the liquid drive. Furthermore, the program describes the motion and regards the inhomogeneities of the different sectors and detects if irregularities appear in the liquid drive.

Measurements have shown that the hardware should stay in the control room due to influencing signals of the electromagnetic field of the MRI if it is placed inside the PET/MRI room. If the lightbarrier system is needed in the final state of the project or if the positioning is possible with the PET data only is part of further investigation. For tests without radiation this system is incessant.

First results of this project have already been presented by Renner et al. [7] at the PSMR conference 2017 in Lisbon. The topic of this speech were the hardware specifications of the PET/MRI head coil system. Results with the phantoms and image reconstruction with this technique will be published in near future.

5 *Conclusion and Outlook*

6 Acknowledgments

I would like to thank all people, who supported me during writing this master thesis. Special thanks to:

- **Prof. Martin Gröschl** for supervising this thesis and correcting it rapidly
- **Prof. Wolfgang Birkfellner** for introducing me into this project as well as giving hints and supporting me during the whole time working here
- **Andreas Renner** not only as colleague in this project but also as a friend and helpful support during the thesis

Last but not least a big thank to **my family** and my girlfriend **Anna** for supporting me throughout the whole studies as well as to all my friends, who gave me the feeling of being at home in Vienna.

6 Acknowledgments

Bibliography

- [1] David Izquierdo-Garcia, Ciprian Catana. *MR Imaging-Guided Attenuation Correction of PET Data in PET/MR Imaging*. PET Clin. (2016)
- [2] Axel Martinez-Möller, Stephan G. Nekolla. *Attenuation correction for PET/MR: Problems, novel approaches and practical solutions* Z. Med.Phys. 22 (2012)
- [3] Gudrun Wagenknecht, Hans-Jürgen Kaiser, Felix M. Mottaghy, Hans Herzog. *MRI for attenuation correction in PET: methods and challenges*. MAGMA (2013)
- [4] Michael Figl, Elmar Laistler, Wolfgang Birkfellner. *Design, Development and Validation of an Integrated Transmission Source System for PET Attenuation Correction in PET/MR Imaging*. FWF project. 2015-2017
- [5] W. Jones, K. Vaigneur, J. Young, J. Reed, C. Moyers, and C. Nahmias. *The Architectural Impact of Single Photon Transmission Measurements on Full Ring 3-D Positron Tomography*. NSS/MIC (1995)
- [6] Navarro de Lara L, Sieg J, Pichler M, Kriegl R, Bogner T, Renner A, Moser E, Beyer T, Birkfellner W, Figl M, and Laistler E. *Development of a head coil system with integrated transmission source for accurate attenuation correction in PET/MRI: RF coil design considerations*. ESMRMB (2016)
- [7] Andreas Renner, Lucia Navarro de Lara, Roberta Frass-Kriegl, Ivo Rausch, Elmar Laistler, Ewald Moser, Thomas Beyer, Wolfgang Birkfellner, Michael Figl (OP5). *A Head Coil System with Integrated Transmission Source for Accurate Attenuation Correction in PET/MRI: Performance Characterization*. PSMR (2017)
- [8] Dominik Dungal. *Optical Tracking of a Transmission Source for PET/MRI Attenuation Correction*. BSc-Thesis TU Wien (2016)
- [9] Dale L Bailey, David W Townsend, Peter E Valk and Michael N Maisey (Eds). *Positron Emission Tomography-Basic Sciences. Chapter 1-2*. Springer-Verlag London Limited (2005)

Bibliography

- [10] J. P. Hornak. *The basics of MRI* copyright 1996-2017,
<https://www.cis.rit.edu/htbooks/mri/inside.htm>, Interactive Learning Software, Henrietta, NY
- [11] Wolfgang Birkfellner, Michael Figl, Johann Hummel. *Medical Image Processing - a basic course*. CRC Press (2011)
- [12] Pichler, B.J., Judenhofer, M.S. & Wehrl, H.F. *PET/MRI hybrid imaging: devices and initial results*. Eur. Radiol. (2008)
- [13] <http://www.schweizer-fn.de/stroemung/druckverlust/druckverlust.php>
Anton Schweizer (07/2017)
- [14] <http://www.druckverlust.de/Online-Rechner/rauh.html> (07/2017)
- [15] Glück, Bernd. *Hydrodynamische und gasdynamische Rohrströmung; Druckverluste Chapter 4*. VEB Verlag für Bauwesen (1988)
- [16] <http://www.cbcity.de/das-kalman-filter-einfach-erklaert-teil-1>
Paul Balzer (05/2013)
- [17] Laser Components. Raytela Polymer Optical Fiber PFU-CD1001-22-E
- [18] <https://www.qt.io/company/>, The Qt Company (2017)
- [19] <https://doc.qt.io/qt-5/qt designer-manual.html>, The Qt Company (2017)
- [20] <https://doc.qt.io/qt-5/signalsandslots.html>, The Qt Company (2017)
- [21] <https://www.qt.io/ide/>, The Qt Company (2017)
- [22] <http://www.medtronic.com/us-en/healthcare-professionals/products/cardiocvascular/cardiopulmonary/bp50-biopump-centrifugal-blood-pump.html>
Medtronic (2017)
- [23] <http://wiki.polymerservice-merseburg.de/index.php/Dichte>

List of Figures

1.1	Tracking of the point source in the liquid drive	2
2.1	Nuclear decay of ^{18}F and electron-positron annihilation of the emitted positron. When emitted by the nucleus the positron starts to lose energy by interactions with other particles until it comes to a resting state. Then it annihilates with an electron to give rise to two photons with an energy of 511 keV each. The photons travel in approximately anti-collinear direction from the annihilation point. [9]	4
2.2	Cross section of a detector ring with a scattered and a random coincidence. One photon of event 1 is scattered which leads to a wrong LOR (dotted line). Event 2 and event 3 are unrelated but result in a LOR as long as they arrive in a coincidence timing window because one photon of each event gets lost.	5
2.3	Different options of implementing a PET detector in a MRI [12]	9
2.4	(A) Comparison of μ -maps between a CT (left) and an ultrashort echo time based MRI (right) and (B) the corresponding PET-image reconstruction. On right side in (B) a comparison of those two methods and their relative change (RC) is visualized. [2]	10
2.5	Coil element layout of the PET/MRI head coil. MRI-FOV is larger than PET-FOV (light-green). Components with high attenuation in PET (red) are outside PET-FOV. The bottom row has only 3 elements to cover the neck in MRI-FOV but also provides space for shoulders [6].	16
2.6	Outer shell with hose system (left) and inner shell (right) of the prototype of the PET/MRI head coil [6].	17
2.7	Lightbarrier block diagram: A LED sends light to the desired position and when the pellet passes by the light intensity at the photodiode changes. This signal is amplified and compared versus a threshold. A micro-controller collects the information and sends it to the PC [8].	17

List of Figures

2.8	Lightbarrier tool with fiber cables. LEDs in the top row provide light to the desired position, the bottom row is receiving the signal if the pellet passes by, turning on the red indicator LEDs. In the back the power supply connection (left cable) and the USB connection (right cable) can be seen [8].	18
3.1	Weir 4000 power supply: Two different outputs (right and left) with a working range of up to 30 V and 2 A. Adjustment is done by turning the knobs. The upper row regulates the voltage, the lower row the current.	22
3.2	BP-50 Bio Pump	22
3.3	Compensating reservoir connected to the hose. The metal part in the middle is removable and deals as sliding guide.	24
3.4	Connecting pieces which act as stoppers of the transmission source on the one hand side and as possibility to disconnect the first part of the liquid drive from the others on the other hand.	25
3.5	On the left side the first arrangement of the direction control is visible. The total distance is slightly different and additional resistance due to the curve is given. In the final arrangement in the right picture these factors are eliminated.	26
3.6	Perfectly filled PMMA pellet in the testing phase. The total length of 24 mm is separated in 2 mm bottom, 10.6 mm of the solution and 4.4 mm of air. Above the screw with a total length of 9.25 mm, 7 mm inside the pellet and 2.25 mm outside are visible.	29
4.1	Time-Voltage relation for the part around the PET/MRI head coil in the liquid drive.	39
4.2	The relationship between time and voltage at the conditions in the PET/MRI room. Especially in the area of turbulent flow the scan duration is higher than in the warmer laboratory.	40
4.3	Deviation of different sectors for different filling volumes at different voltages. Sector 1 is always marked in blue, sector 2 in red, sector 3 in green and sector 4 is the violet dot in each plot. “thin” means the sharp end of the pellet is in front of the motion, while “thick” implies the same for the flat.	47
4.4	Quarter coefficients for the different sectors at a voltage of 2 V. (a) represents the values with the thin end frontwards, (b) shows the results for the thick end frontwards.	49
4.5	Quarter coefficients for the different sectors at a voltage of 4 V. (a) represents the values with the thin end frontwards, (b) shows the results for the thick end frontwards.	49

4.6 Quarter coefficients for the different sectors at a voltage of 10 V. (a) represents the values with the thin end frontwards, (b) shows the results for the thick end frontwards. 50

4.7 Effect of the torsional momentum on the pellet motion. Indirect proportionality of the quarter coefficients is given because it leads to promotion in one direction while it constrains the movement in the other way. (a) shows the correction coefficients with the thick end frontwards, while (b) presents the reciprocal correction coefficient of the thin end frontwards. 51

4.8 Average normalized round times with its standard deviation for a voltage of 2V. (a) represents the thin end of the pellet frontwards, (b) the results with the thick end. 53

4.9 Average normalized round times with its standard deviation for a voltage of 4V. (a) represents the thin end of the pellet frontwards, (b) the results with the thick end. 53

4.10 Average normalized round times with its standard deviation for a voltage of 10V. (a) represents the thin end of the pellet frontwards, (b) the results with the thick end. 53

4.11 Upper part of the GUI after starting the software of the lightbarrier system 56

4.12 Upper part of the “Cable Positions” dialog 56

4.13 The “Initial Parameters” dialog of the lightbarrier system 58

List of Figures

List of Tables

2.1	Comparison of attenuation coefficients μ for 511 keV photons in different tissue [9]	6
2.2	Kinematic viscosity ν of water at different temperatures T for a pressure of 1bar. The table is adapted to the room temperature in the laboratory.	12
3.1	Components of the liquid drive. The second column gives the number n how often the component is used in the liquid drive and the last column the pressure loss coefficient ζ	27
3.2	α -values of components where the diameter decreases.	27
3.3	Parameters which are taken into account for the pellet choice. Length l and diameter d must consider the diameter of the tube and the radius of the PET/MRI head-coil. The inner height is the result of length minus bottom strength and screw length.	28
3.4	Resulting volumes for the pellets described in Table 3.3. In the second column shows the total available volume V , beside it the perfect filling volume V_{H_2O} for floating in the testing phase with distilled water and in the last column the perfect filling volume V_{D_2O} for floating in the final state with heavy water in the liquid drive are present.	28
3.5	Densities of materials used for volume calculations of the pellet. . .	29
4.1	Summary of the main parameters used for further measurements. Results of measurements from Section 4.5 are also taken into account for these results	39
4.2	Loss of pressure δp for the maximum flow volume of the pump. In this case the flow in all segments is turbulent (t).	41
4.3	Loss of pressure δp in the fast scanning mode at 10 V. Turbulent flow (t) exists in this case as well as a mixture of turbulent and laminar flow (m).	41
4.4	Loss of pressure δp in the transmission scan mode at 4 V. The flow is laminar l for all components in this case.	41

List of Tables

4.5	Loss of pressure δp in the blank scan mode at 2 V. The flow is laminar l for all components in this case.	42
4.6	Comparison between distances l in [m] and round segments in [°] .	43
A.1	Time-Voltage relation in the laboratory	76
A.2	Time-Voltage relation in the PET/MRI room.	76
A.3	Results for a filling volume of 200 μl and the thin end frontwards. .	77
A.4	Results for a filling volume of 200 μl and the thick end frontwards. .	77
A.5	Results for a filling volume of 250 μl and the thin end frontwards. .	78
A.6	Results for a filling volume of 250 μl and the thick end frontwards. .	78
A.7	Results for a filling volume of 300 μl and the thin end frontwards. .	78
A.8	Results for a filling volume of 300 μl and the thick end frontwards. .	79
A.9	Results for a filling volume of 350 μl and the thin end frontwards. .	79
A.10	Results for a filling volume of 350 μl and the thick end frontwards. .	79
A.11	Results for a filling volume of 400 μl and the thin end frontwards. .	80
A.12	Results for a filling volume of 400 μl and the thick end frontwards. .	80
A.13	Quarter coefficients for 2 V and the thick end in front.	80
A.14	Quarter coefficients for 2 V and the thin end in front.	81
A.15	Quarter coefficients for 4 V and the thick end in front.	81
A.16	Quarter coefficients for 4 V and the thin end in front.	81
A.17	Quarter coefficients for 10 V and the thick end in front.	82
A.18	Quarter coefficients for 10 V and the thin end in front.	82
A.19	Round coefficients for 2 V movement with the thin end in front . .	83
A.20	Round coefficients for 2 V movement with the thick end in front . .	84
A.21	Round coefficients for 4 V movement with the thin end in front . .	84
A.22	Round coefficients for 4 V movement with the thick end in front . .	85
A.23	Round coefficients for 10 V movement with the thin end in front . .	85
A.24	Round coefficients for 10 V movement with the thick end in front .	86

List of Abbreviations

PET	Positron Emission Tomography
CT	Computer Tomography
MRI/MRT	Magnetic Resonance Imaging
AC	Attenuation Correction
FWF	Fonds zu Förderung der wissenschaftlichen Forschung
Tx	Transmission
FDG	Fluorodeoxyglucose
LOR	Line of Response
RF	Radion Frequency
FID	Free Induction Decay
FOV	Field of View
LED	Light-emitting Diode
GUI	Graphical User Interface
IDE	Integrated Development Environment
PMMA	Polymethymethacylat

A Appendix

A.1 Time/Voltage comparison

Voltage [V]	Time [s]	Voltage [V]	Time [s]	Voltage [V]	Time [s]
2,04	869,81	6,08	118,55	12,5	44,67
2,04	838,08	6,11	118,03	12,53	44,6
2,29	680,05	6,45	111	12,56	44,18
2,5	589,29	6,47	111	12,62	44
2,52	553	7,01	100	12,66	44
2,68	491,79	7,02	97	12,71	43,47
2,68	479,38	7,56	88	12,71	43,24
2,77	470,82	7,56	86	12,72	43,07
2,77	462,44	7,98	82	12,74	42,95
3,06	374,22	7,98	82	12,77	42,72
3,06	367,96	8,13	81	12,8	42,39
3,06	354,54	8,14	79	13,1	42,16
3,3	313,51	8,55	75	13,1	41,68
3,32	308	8,56	73	13,1	41,49
3,43	305,7	8,94	69	13,13	41,4
3,44	300,03	9,04	69	13,16	41,33
3,61	262,27	9,48	65	13,47	40,35
3,61	261,48	9,48	64	13,71	39,63
3,61	257,39	9,7	63	13,89	38,03
3,98	230,7	9,72	62	14,22	37,99
4,01	226,23	10,01	60,63	14,28	36,77
4,02	226,19	10,02	60	14,66	36,73
4,03	223,71	10,08	59,86	14,66	35,99
4,03	222,85	10,08	59	14,88	35,88
4,1	220,16	10,5	56	15,02	35,82
4,44	190,3	10,54	55	15,02	35,33
4,52	188,42	10,98	54	15,02	34,16
4,54	187,47	11,02	54	15,42	34,04

A Appendix

4,54	184,66	11,48	51	15,45	33,85
4,54	183,63	11,54	49	15,46	33,08
4,57	183,6	11,63	48,59	15,66	33
4,96	158,59	11,64	48,1	15,81	32,6
5	157,5	11,79	48	16,22	31,5
5,08	156,3	11,79	47,84	16,25	31,48
5,08	154,92	11,81	47,56	16,77	31,24
5,09	154,86	11,81	47,55	16,83	30,55
5,09	154,24	11,93	47	17,17	30
5,38	138,04	11,96	47	17,23	29,84
5,53	134,66	12,02	46,86	17,53	29,65
5,56	134,24	12,05	46,59	17,89	28,99
5,56	133	12,09	45,87	17,89	28,49
5,96	120,17	12,15	45,52	18,66	27
6,04	120	12,17	45,37	18,7	27
6,06	120	12,2	45,14		
6,08	119,5	12,22	44,89		

Table A.1: Time-Voltage relation in the laboratory

Voltage [V]	Time [s]	Voltage [V]	Time [s]
1,8	1229	6,11	118
2,2	824	8,56	83,5
3,31	310	8,7	82,7
4,57	184	8,96	81
5,08	155	9,03	79
6,08	118		

Table A.2: Time-Voltage relation in the PET/MRI room.

A.2 Filling

thin	Voltage/Quarter	CD	DA	AB	BC
	2,06	-10,42	-13,99	6,85	17,56
	3,07	-2,75	-4,90	2,84	4,81
	3,58	-1,62	-3,01	1,51	3,11
	4,03	-1,44	-2,08	1,25	2,27
	4,54	-1,04	-1,61	0,91	1,75
	5,07	-0,22	-1,69	0,16	1,75
	5,59	-0,31	-0,70	-0,33	1,33
	6,08	-0,32	-0,45	-0,19	0,96

Table A.3: Results for a filling volume of 200 μl and the thin end frontwards.

thick	Voltage/Quarter	CB	BA	AD	DC
	3,07	-3,39	-2,85	2,92	3,32
	3,58	-3,32	-1,74	3,01	2,05
	4,03	-2,19	-1,24	1,92	1,51
	4,54	-2,05	-1,00	1,74	1,32
	5,07	-2,02	-0,74	1,88	0,88
	5,59	-1,49	-0,38	0,80	1,07
	6,08	-1,29	-0,23	0,91	0,61

Table A.4: Results for a filling volume of 200 μl and the thick end frontwards.

A Appendix

thin	Voltage/Quarter	CD	DA	AB	BC
	2,06	-5,06	-4,60	3,42	6,23
	3,07	-1,47	-1,42	0,71	2,18
	3,58	0,48	-1,01	0,27	0,26
	4,03	-0,61	-0,44	0,35	0,70
	4,54	-0,49	-0,50	0,39	0,59
	5,07	-0,75	0,75	0,06	-0,07
	5,59	-0,87	-0,05	0,78	0,14
	6,08	-0,85	0,92	0,16	-0,22

Table A.5: Results for a filling volume of 250 μl and the thin end frontwards.

thick	Voltage/Quarter	CB	BA	AD	DC
	3,07	-2,58	1,62	1,50	-0,55
	3,58	-3,38	1,57	2,63	-0,82
	4,03	-2,79	0,53	2,85	-0,59
	4,54	-2,29	0,80	2,04	-0,55
	5,07	-2,07	0,52	1,49	0,06
	5,59	-2,19	0,44	2,13	-0,38
	6,08	-2,11	0,93	1,80	-0,62

Table A.6: Results for a filling volume of 250 μl and the thick end frontwards.

thin	Voltage/Quarter	CD	DA	AB	BC
	2,06	3,52	3,53	-4,37	-2,68
	3,07	0,95	1,93	-1,33	-1,55
	3,58	0,47	1,95	-0,70	-1,72
	4,03	0,39	0,91	-0,30	-0,99
	4,54	0,39	1,41	-1,43	-0,37
	5,07	0,20	0,78	0,12	-1,10
	5,59	0,07	1,07	-0,96	-0,19
	6,08	-0,40	1,02	0,11	-0,73

Table A.7: Results for a filling volume of 300 μl and the thin end frontwards.

thick	Voltage/Quarter	CB	BA	AD	DC
	3,07	-1,14	3,06	1,15	-3,07
	3,58	-0,48	2,94	-0,81	-1,66
	4,03	-1,87	1,82	1,55	-1,50
	4,54	-2,54	1,59	1,20	-0,25
	5,07	-2,30	1,01	1,96	-0,67
	5,59	-1,93	0,64	1,82	-0,53
	6,08	-2,65	1,19	2,13	-0,67

Table A.8: Results for a filling volume of 300 μl and the thick end frontwards.

thin	Voltage/Quarter	CD	DA	AB	BC
	2,06	3,52	3,53	-4,37	-2,68
	3,07	0,95	1,93	-1,33	-1,55
	3,58	0,47	1,95	-0,70	-1,72
	4,03	0,39	0,91	-0,30	-0,99
	4,54	0,39	1,41	-1,43	-0,37
	5,07	0,20	0,78	0,12	-1,10
	5,59	0,07	1,07	-0,96	-0,19
	6,08	-0,40	1,02	0,11	-0,73

Table A.9: Results for a filling volume of 350 μl and the thin end frontwards.

thick	Voltage/Quarter	CB	BA	AD	DC
	3,07	-1,14	3,06	1,15	-3,07
	3,58	-0,48	2,94	-0,81	-1,66
	4,03	-1,87	1,82	1,55	-1,50
	4,54	-2,54	1,59	1,20	-0,25
	5,07	-2,30	1,01	1,96	-0,67
	5,59	-1,93	0,64	1,82	-0,53
	6,08	-2,65	1,19	2,13	-0,67

Table A.10: Results for a filling volume of 350 μl and the thick end frontwards.

A Appendix

thin	Voltage/Quarter	CD	DA	AB	BC
	2,06	8,01	9,93	-7,08	-10,86
	3,07	2,03	5,41	-2,16	-5,29
	3,58	1,12	2,64	-0,57	-3,19
	4,03	1,01	2,85	-0,97	-2,89
	64,54	0,54	2,03	-0,34	-2,24
	5,07	0,08	1,44	-0,13	-1,39
	5,59	0,20	1,43	-0,13	-1,49
	6,08	-0,32	2,10	-0,25	-1,53

Table A.11: Results for a filling volume of 400 μl and the thin end frontwards.

thick	Voltage/Quarter	CB	BA	AD	DC
	3,07	1,11	4,50	-0,31	-5,31
	3,58	0,20	3,07	0,42	-3,70
	4,03	-0,41	2,81	0,84	-3,23
	4,54	-1,08	2,27	1,38	-2,56
	5,07	-1,09	1,64	1,48	-2,04
	5,59	-1,20	1,57	1,24	-1,61
	6,08	-1,62	1,28	2,00	-1,65

Table A.12: Results for a filling volume of 400 μl and the thick end frontwards.

A.3 Quarter coefficients

Value/Sector	1	2	3	4
Minimum	0,954	0,922	0,968	0,969
Quartil 1	1,019	0,950	0,997	0,995
Median	1,029	0,957	1,007	1,008
Quartil 3	1,046	0,967	1,016	1,019
Maximum	1,104	1,041	1,048	1,054

Table A.13: Quarter coefficients for 2 V and the thick end in front.

A.3 Quarter coefficients

Value/Sector	1	2	3	4
Minimum	0,981	1,036	0,936	0,851
Quartil 1	1,027	1,067	0,977	0,890
Median	1,039	1,081	0,991	0,905
Quartil 3	1,054	1,091	1,008	0,918
Maximum	1,113	1,133	1,046	0,968

Table A.14: Quarter coefficients for 2 V and the thin end in front.

Value/Sector	1	2	3	4
Minimum	0,996	0,965	0,918	0,962
Quartil 1	1,011	0,980	0,993	0,989
Median	1,020	0,986	0,999	0,997
Quartil 3	1,029	0,993	1,006	1,005
Maximum	1,039	1,013	1,025	1,050

Table A.15: Quarter coefficients for 4 V and the thick end in front.

Value/Sector	1	2	3	4
Minimum	0,963	1,003	0,970	0,929
Quartil 1	0,997	1,019	0,997	0,956
Median	1,004	1,027	1,010	0,962
Quartil 3	1,015	1,033	1,021	0,969
Maximum	1,035	1,071	1,043	0,992

Table A.16: Quarter coefficients for 4 V and the thin end in front.

A Appendix

Value/Sector	1	2	3	4
Minimum	0,967	0,980	0,997	0,976
Quartil 1	0,986	0,991	1,006	0,994
Median	0,994	0,996	1,010	1,001
Quartil 3	0,999	1,002	1,015	1,007
Maximum	1,011	1,019	1,031	1,017

Table A.17: Quarter coefficients for 10 V and the thick end in front.

Value/Sector	1	2	3	4
Minimum	0,951	0,996	0,977	0,958
Quartil 1	0,997	1,011	0,991	0,974
Median	1,003	1,016	0,998	0,983
Quartil 3	1,009	1,023	1,006	0,991
Maximum	1,036	1,065	1,021	0,999

Table A.18: Quarter coefficients for 10 V and the thin end in front.

A.4 Round movement

Round	Coefficient	Deviation
1	1,013	0,034
2	1,009	0,019
3	1,018	0,028
4	1,001	0,023
7	1,004	0,022
8	1,017	0,028
9	1,009	0,020
11	1,005	0,021
12	0,999	0,030
13	0,989	0,028
16	0,988	0,012
17	1,003	0,020
18	0,982	0,036
19	0,987	0,046
20	1,002	0,035

Table A.19: Round coefficients for 2 V movement with the thin end in front

A Appendix

Round	Coefficient	Deviation
1	1,019	0,034
2	1,001	0,034
3	1,016	0,037
4	0,997	0,019
7	0,992	0,022
8	0,998	0,029
9	1,008	0,030
11	0,995	0,026
12	0,996	0,024
13	0,995	0,021
16	1,000	0,017
17	1,013	0,031
18	1,015	0,036
19	0,992	0,034
20	0,997	0,029

Table A.20: Round coefficients for 2 V movement with the thick end in front

Round	Coefficient	Deviation
1	1,010	0,016
2	1,007	0,012
3	1,000	0,011
4	1,003	0,014
7	0,995	0,015
8	0,998	0,007
9	1,000	0,013
11	1,004	0,013
12	1,002	0,009
13	0,999	0,011
16	1,001	0,009
17	1,001	0,012
18	1,003	0,009
19	0,994	0,011
20	0,991	0,008

Table A.21: Round coefficients for 4 V movement with the thin end in front

Round	Coefficient	Deviation
1	1,008	0,013
2	1,013	0,011
3	1,006	0,013
4	0,995	0,011
7	1,001	0,009
8	1,004	0,011
9	0,997	0,009
11	0,999	0,006
12	1,003	0,011
13	0,992	0,015
16	0,995	0,008
17	1,001	0,008
18	0,995	0,009
19	0,998	0,010
20	1,005	0,011

Table A.22: Round coefficients for 4 V movement with the thick end in front

Round	Coefficient	Deviation
1	1,004	0,006
2	1,000	0,005
3	0,996	0,004
4	0,996	0,004
7	0,995	0,005
8	1,002	0,004
9	1,001	0,006
11	1,004	0,002
12	1,005	0,005
13	1,001	0,004
16	0,998	0,004
17	1,007	0,005
18	1,009	0,005
19	0,996	0,006
20	0,997	0,007

Table A.23: Round coefficients for 10 V movement with the thin end in front

Round	Coefficient	Deviation
1	1,005	0,007
2	0,999	0,006
3	1,011	0,006
4	1,005	0,007
7	1,003	0,004
8	0,999	0,004
9	1,005	0,004
11	1,000	0,004
12	0,971	0,012
13	1,026	0,017
16	0,995	0,003
17	0,996	0,004
18	0,996	0,004
19	1,001	0,006
20	0,994	0,006

Table A.24: Round coefficients for 10 V movement with the thick end in front

A.5 Code segments

A.5.1 MuckData

Code segment A.1: Selection of the right timestamps of the `DetectionData`.

The example shows the code in frontwards direction (`direction=true`) for the thin end frontwards (`pelletend=true`)

```

if(pelletend==true)
{
    for(int i=0; i < DetectionData.size()-3; i+=3)
    {
        if(DetectionData[i+3]==DetectionData[i])
        {
            continue;
        }
        else
        {
            PosTime.append(DetectionData[i]);
        }
    }
}

```

```

        PosTime.append(DetectionData[i+1]);
        PosTime.append(DetectionData[i+2]);
    }
}
PosTime.append(DetectionData[DetectionData.size()-3]);
PosTime.append(DetectionData[DetectionData.size()-2]);
PosTime.append(DetectionData[DetectionData.size()-1]);
}

if(direction==true)
{
    for(int i=0; i < newpos.size()-1; i+=1)
    {
        if(newpos[i+1]==newpos[i])
        {
            continue;
        }
        else
        {
            cabpos.append(100*newpos[i]);
        }
    }

    for(int i=0; i < allSpeed.size()-1; i+=1)
    {
        if(allSpeed[i]==0 || allSpeed[i+1]==allSpeed[i])
        {
            continue;
        }
        else
        {
            Speed.append(allSpeed[i]);
        }
    }
    cabpos.append(100*newpos[newpos.size()-1]);

    if(allSpeed[allSpeed.size()-1]!=0)
    {
        Speed.append(allSpeed[allSpeed.size()-1]);
    }
}

```

```
    if(cabpos.size() < 16)
    {
        for(int i=cabpos.size(); i < 16; i++)
        {
            cabpos.append(cabpos[cabpos.size() - 1]);
        }
    }
}
```

A.5.2 Output Data

Code segment A.2: Data in the output file. First the initial parameters are given followed by the detected positions and then all positions of the pellet with its timestamp. In the end other important parameters are listed.

```
stream << "Voltage ,_Direction(true=frontwards) ,
pelletend_(true=thin)" << endl;
stream << voltage << ",_" << direction << ",_"
    << pelletend << endl;

stream << "Time_needed_in_ms:" << ",_" << totTime << endl;

stream << "Position ,_Time[us] ,_SystemTime[ms]" << endl;
for(int i=0; i < PosTime.size(); i+=3)
{
    stream << PosTime[i] << ",_" << PosTime[i+1] << ",_"
        << PosTime[i+2] << endl;
}

stream << "Position ,_Time ,_Lightbarrier_Time ,_actual_velocity"
    << endl;
for(int l=0; l < ActPos.size(); l++)
{
    stream << ActPos[l] << ",_" << actCompTime[l] << ",_"
        << actSysTime[l] << ",_" << actVel[l] << endl;
}

stream << "Position" << endl;
```

```

for (int i=0; i < cabpos.size (); i++)
{
    stream << cabpos[i] << endl;
}

stream << "Round_Time" << ",_" << "degrees_at_start" << ",_"
    << "degrees_at_end" << endl;
for(int i=0; i< roundTime.size (); i+=3)
{
    stream << roundTime[i] << ",_" << roundTime[i+1] << ",_"
        << roundTime[i+2] << endl;
}

stream << "Quarter_1" << ",_" << "degrees_at_start" << ",_"
    << "degrees_at_end" << endl;
for(int i=0; i< quarter1Time.size (); i+=3)
{
    stream << quarter1Time[i] << ",_" << quarter1Time[i+1] << ",_"
        << quarter1Time[i+2] << endl;
}
...

stream << "Coefficient_1" << endl;
for(int i=0; i<Coefficient1.size (); i++)
{
    stream << Coefficient1[i] << endl;
}
...

stream << "Positions:" << endl;
for(int j=0; j < Position.size (); j++)
{
    stream << Position[j] << endl;
}

stream << "Velocity" << endl;
for (int i=0; i< Velocity.size (); i++)
{
    stream << Velocity[i] << ",_"<< realposition[i] << ",_"
        << realtime[i] <<endl;
}

```

A Appendix

```
}  
  
stream << "final_coefficients_1-4" << endl;  
for(int i=0; i<quarterCoeff.size(); i++)  
{  
    stream << quarterCoeff[i] << endl;  
}  
...  
}
```
